© 2014. Published by The Company of Biologists Ltd | Development (2014) 141, 2483-2493 doi:10.1242/dev.108662

RESEARCH ARTICLE

A regulatory receptor network directs the range and output of the Wingless signal

Sabine Schilling*,‡, Sarah Steiner‡, Dario Zimmerli‡ and Konrad Basler§

ABSTRACT

The potent activity of Wnt/Wingless (Wg) signals necessitates sophisticated mechanisms that spatially and temporally regulate their distribution and range of action. The two main receptor components for Wg – Arrow (Arr) and Frizzled 2 (Fz2) – are transcriptionally downregulated by Wg signaling, thus forming gradients that oppose that of Wg. Here, we analyze the relevance of this transcriptional regulation for the formation of the Wg gradient in the *Drosophila* wing disc by combining *in vivo* receptor overexpression with an *in silico* model of Wg receptor interactions. Our experiments show that ubiquitous upregulation of Arr and Fz2 has no significant effects on Wg output, whereas clonal overexpression of these receptors leads to signaling discontinuities that have detrimental phenotypic consequences. These findings are supported by our *in silico* model for Wg diffusion and signal transduction, which suggests that abrupt changes in receptor levels causes discontinuities in Wg signaling. Furthermore, we identify a 200 bp regulatory element in the *arr* locus that can account for the Arr gradient, and we show that this is indirectly negatively controlled by Wg activity. Finally, we analyze the role of Frizzled 3 (Fz3) in this system and find that its expression, which is induced by Wg, contributes to the establishment of the Arr and Fz2 gradients through counteracting canonical signaling. Taken together, our results provide a model in which the regulatory network of Wg and the three receptor components account for the range and shape of this prototypical morphogen system.

KEY WORDS: Wingless receptors, Wnt pathway, Model for Wg diffusion

INTRODUCTION

Communication between the cells in a tissue depends on extracellular signaling molecules. The vast majority of these are produced by defined subsets of cells. This restricted production provides spatial information that is needed for the signals to orchestrate patterning and growth. The signaling output is dependent on the range of action and level of activity of the secreted signaling protein – determinants that depend not only on the biochemical nature of the signal but also on the receptor systems that are employed by the receiving cells. The glycoproteins of the Wnt family serve as an interesting model to understand the interplay between these determinants.

Mechanisms that precisely and tightly control Wnt signal reception and transduction, both spatially and temporally, are absolutely necessary – Wnt signaling is crucial in many developmental processes, and improper activation of the canonical signaling cascade can have severe pathological consequences, such as cancer (Clevers, 2006). Altering receptor levels is often the first step in attenuating the cellular response to a signaling molecule. Receptor downregulation can be achieved on the transcriptional level through repression of the receptor-encoding gene, or on the protein level through internalization and subsequent lysosomal degradation. Both processes lead to a diminution of active receptors from the cell membrane and, thereby, to an attenuation of the signaling output.

Wingless (Wg), the founding member of the highly conserved Wnt family, plays an important role in the primordium of the *Drosophila melanogaster* wing (Zecca et al., 1996; Neumann and Cohen, 1997). In this tissue, Wg is expressed in a thin stripe at the dorsal-ventral boundary from where it spreads to either side, producing a symmetrical concentration gradient. The canonical Wnt/Wg transduction pathway is initiated by the binding of Wnt/Wg ligands to a receptor of the Frizzled family and a co-receptor, the low-density lipoprotein receptor-related LRP5/6 [Arrow (Arr) in *D. melanogaster*]. This binding transduces the extracellular signal into an intracellular cascade that ultimately results in the cytoplasmic stabilization and nuclear localization of β-catenin/Armadillo (Arm) and its subsequent association with TCF/LEF [Pangolin (Pan) in *D. melanogaster*] DNA binding proteins. The activation of Wnt target genes is promoted by the interaction of the bipartite Arm-Pan complex with various auxiliary co-factors (Mosimann et al., 2009).

In *Drosophila*, the genes encoding the Wg receptor Fz2 and the co-receptor Arr are transcriptionally downregulated by Wg signaling (Cadigan et al., 1998; Wehrli et al., 2000). However, the details of the underlying molecular mechanism, and an understanding of its physiological significance, are still lacking. Wnt-induced transcriptional repression could be either direct or indirect; only a detailed analysis of the *cis*-regulatory elements (CREs) and the corresponding transcription factors can distinguish between these modes of repression (Affolter et al., 2008). In addition to signaling-induced transcriptional downregulation, there is evidence for a collateral post-transcriptional layer of regulation of Wg receptors. Both Fz2 and Arr contain endocytosis signals and have been shown to localize to endocytic compartments together with their ligand Wg (Rives et al., 2006), which suggests that both the receptor and co-receptor are internalized upon Wg binding. The contribution of this to Wg internalization, however, is less clear, as it can also occur in their absence (Baeg et al., 2004).

Here, we experimentally address the contribution of the transcriptional regulation of the Wg receptors Arr and Fz2 to wing development and Wg gradient formation. We show that Wg-mediated patterning is, remarkably, unaffected by a ubiquitous upregulation of the levels of the receptor. However, local interruptions of the transcriptional gradient of *arr* and *fz2* lead to detrimental outcomes caused by an imbalance between receptor and ligand levels at the borders of signaling discontinuity. Furthermore, we uncover a second, but less important, layer of control – in high-signaling regions the decoy receptor Fz3 is expressed, dampening the signal. By dissecting

Institute of Molecular Life Sciences, University of Zurich, 8057 Zurich, Switzerland.
*Present address: Institute of Molecular Systems Biology, ETH Zurich, 8093 Zurich, Switzerland.
‡These authors contributed equally to this work

§Author for correspondence (basler@imls.uzh.ch)

Received 7 February 2014; Accepted 24 April 2014

Development (2014) 141, 2483-2493 doi:10.1242/dev.108662

the regulatory control regions that are responsible for *arr* and *fz3* expression, we find *fz3* to be a direct positive, and *arr* an indirect negative, target of the Wg pathway.

RESULTS

Transcriptional downregulation of Arr and Fz2 by Wg signaling

In the *Drosophila melanogaster* wing imaginal disc, the expression pattern of Arr and the inferred Wg protein gradient are inverse (Fig. 1A-C) – low Arr levels close to the Wg source are contrasted by high Arr levels at sites of little or no Wg. We explored the potential relevance of the Arr expression pattern by experimentally perturbing it, by using a heterologous ubiquitously active promoter. Surprisingly, animals that expressed Arr under the control of the *tubulinα1* promoter (*tubArr*) were viable and did not show any wing phenotypes. To monitor Arr expression in *tubArr* animals, we used an antibody against Arr for immunohistochemical analysis. Arr expression was elevated in *tubArr* wing pouches, but still graded, with reduced levels towards the Wg expression domain (Fig. 1D-F). We quantified the fluorescent intensities of Arr in *tubArr* and

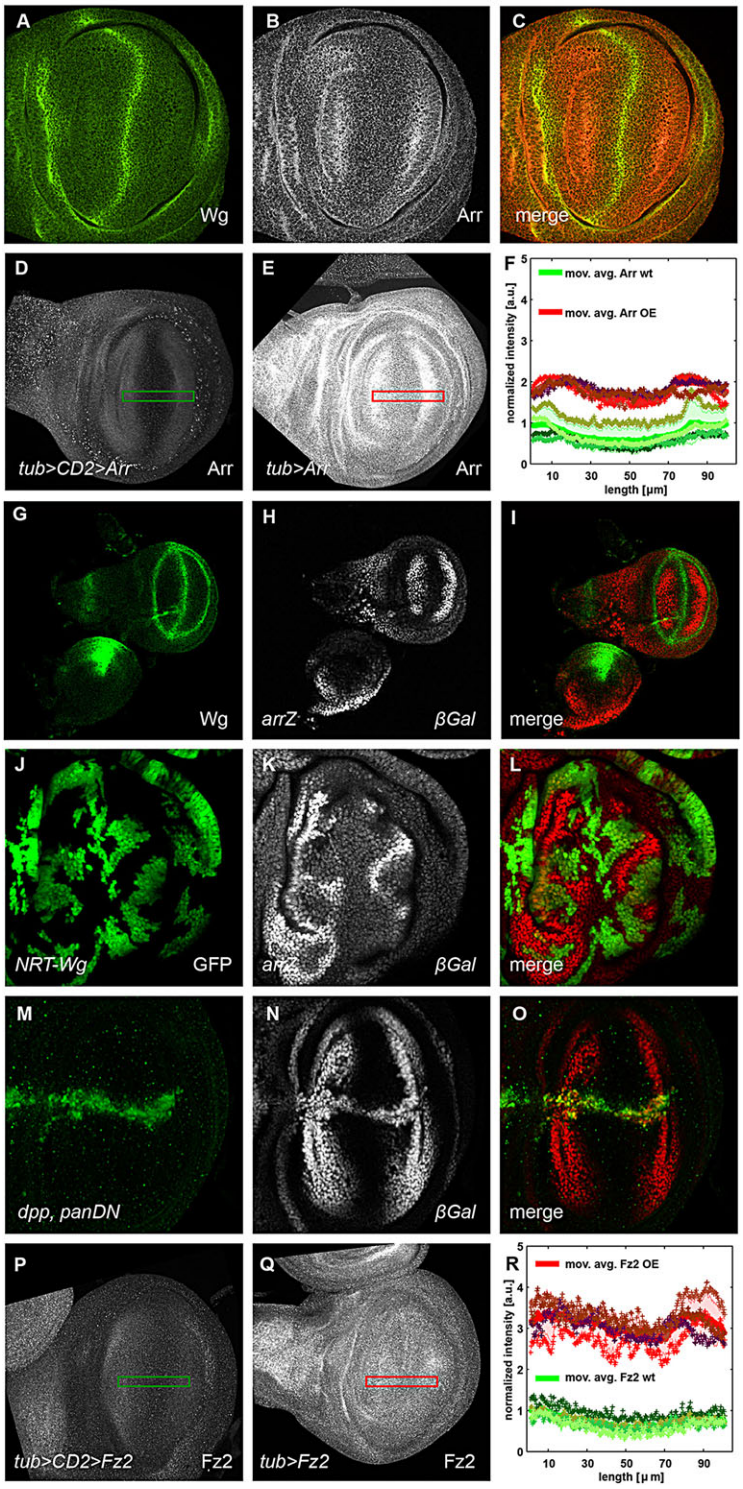

Fig. 1. Wg represses its receptors Arrow and Frizzled 2 – graded expression of the receptors is maintained upon *tubulinα1* promoter-mediated misexpression. In all panels showing imaginal discs, the posterior compartment is oriented towards the top, the anterior compartment is towards the bottom of the image. The green (D,P) and red (E,Q) rectangles displayed on these example discs show the ROI, sized 100 µm×16 µm, that was used to quantify the level of receptor in F and R. (A-C) Wingless (Wg) and Arrow (Arr) exhibit an inverse relationship in their expression levels. Immunofluorescence staining for Wg (green in A and C) and Arr (gray in B and red in C) revealed the inverse expression levels of the two proteins (C). (D,E) Graded Arr expression was maintained in Arr-overexpressing discs. Wild-type wing discs (D), and wing discs that misexpressed Arr, controlled by the *tubulinα1* promoter (tubArr) (E), were stained for Arr. (G-L) Wg represses *arr* transcription. The transcriptional *arr* reporter *arr-lacZ* (*arrZ*) (gray, H) was repressed in Wg-expressing areas of the wing imaginal disc. It was also repressed in randomly induced somatic clones (gray, K), as revealed by immunostaining against β-galactosidase (β-Gal), that overexpressed membrane-attached NRT-Wg [marked by green fluorescent protein (GFP) in J]. (M-O) Dominant-negative pan (panDN) derepresses Arr. Expression of dominant-negative *UAS-panDN* with *dppGAL4* (M), marked by GFP, led to derepression of the *arrZ* reporter (gray, N). (P,Q) Graded Fz2 expression is maintained in Fz2-overexpressing discs. *tubFz2*-expressing wing discs (Q) that were immunostained for Fz2 showed a higher intensity profile of Fz2 than that of wild-type controls (P). Note that the receptor upregulation in *tubFz2* was much stronger than in the corresponding *tubArr* discs. (F,R) Receptor level intensity plots. In both panels, intensities of four wild-type (wt, green-shaded crosses) and four receptor-overexpressing discs (OE, red-shaded crosses) are projected on the longer axis of the ROI, perpendicular to the dorsal-ventral compartment boundary. The corresponding moving averages (defined by a half window size of three micrometer) are denoted by solid green (wt) and red (overexpression) lines. Green- and red-shaded areas denote standard deviations of the mean of the data from wild-type and mutant imaginal discs, respectively. Intensity plots were normalized to the maximum of the moving average of the wild-type discs. a.u., arbitrary units.

Development (2014) 141, 2483-2493 doi:10.1242/dev.108662

control animals. The absolute Arr levels in *tubArr* animals were higher, whereas the shapes of the gradients were similar to those in the wild type (Fig. 1F; supplementary material Table S1).

In order to further analyze the *arr* transcriptional gradient, we used the recessive lethal *lacZ* P-element insertion *l(2)k08131*, which we refer to as *arrZ* (Wehrli et al., 2000) and is uncharacterized at the molecular level. We mapped the insertion site and found that it is positioned in the 5′UTR region of *arr* in the short first untranslated exon (data not shown). Owing to its insertion site and its expression pattern, *arrZ* can be used as a molecular read-out to study the transcription of the *arr* gene. *arrZ* is expressed in a graded manner and is inactive in areas of high Wg signaling (Fig. 1G-I). To investigate this negative regulation of *arr* by Wg, we clonally overexpressed NRT-Wg, which is a membrane-tethered non-diffusible fusion protein of Wg (Zecca et al., 1996). All over the wing imaginal disc, clones that expressed *NRT-Wg* showed repression of *arrZ*, as did adjacent wild-type neighboring cells (Fig. 1J-L). We next asked whether the nuclear mediator of Wg signaling Pan is involved in *arrZ* repression. Overexpression of a dominant-negative form of Pan (*UAS-panDN-HA*), which lacks the Armadillo-binding domain and was tagged with hemagglutinin (HA), resulted in a strong and strictly cell-autonomous derepression of *arrZ* expression (Fig. 1M-O). Hence, *arrZ* is a negative target of Wg signaling in the wing pouch and is repressed as a consequence of signaling events downstream of Pan.

Negative transcriptional regulation by Wg signaling has also been reported for the *fz2* gene, which encodes the main Wg receptor (Cadigan et al., 1998). To study the physiological relevance of this regulation, we misexpressed Fz2 under the control of the *tubulinα1* promoter (*tubFz2*) in the wing imaginal disc. Similar to the case of *tubArr*, *tubFz2* animals had wings that appeared wild type. Also, as observed for Arr, Fz2 protein levels were elevated in *tubFz2* animals, but remained graded with a slightly steeper slope, as observed for that in corresponding wild-type discs (Fig. 1P-R; supplementary material Table S1). Although weaker, a gradient could still be observed in larvae that harbored *tubFz2* but lacked endogenous Fz2 (supplementary material Fig. S1A-D and Table S1). These observations suggest that post-transcriptional regulation plays a rather minor role in gradient formation.

Modeling Wg receptor interactions

To formalize, and systematically study, the mechanisms of Wg-receptor interaction, we developed an *in silico* model that reproduces the negative regulation of Arr and Fz2 by Wg in cells of the wing pouch (Fig. 2). We first reduced the complexity of the system by summarizing the similar biological roles of the receptor Arr and its co-receptor Fz2 into the receptor entity ‘ArrFz2’. Next, we set up a system of coupled ordinary and partial differential equations that described the production and decay of the Wg ligand and its receptors, the reverse complex formation between ligand and the receptor entity, the diffusion of Wg, as well as the transcriptional downregulation of the receptor entity by Wg (Fig. 2).

A simplified analytical model suggests that most Wg is not bound to its receptors

Neglecting the Wg-induced transcriptional receptor repression ($k^t_{Wg-ArrFz2}=0$ in Fig. 2) allowed us to study the effect of receptor upregulation analytically in one dimension (Schwank et al., 2011; details in the supplementary methods). Supplementary material Fig. S2 shows the dependence of the amplitude of total Wg (black) in regions that overexpressed the receptor on the relative amount of ligand that was not bound to the receptor, $a=[Wg]/[Wg_T]$. In such a simplified model, the higher the value of a, the less the amplitude of the total Wg distribution is affected by changes in receptor levels.

To study the consequences of apposing wild-type and receptor-overexpressing cells, as well as to have a direct comparison of the Wg distribution in receptor-overexpressing cells to wild-type cells in the same disc, we generated *tubulinα1>CD2,y⁺>arr* and *tubulinα1>CD2,y⁺>fz2* transgenes that harbored flp-out cassettes between the promoter and coding region. Exposure to Flp recombinase during development leads to clones that overexpress the corresponding receptor. In discs, where the receptor overexpression was compartmental (Fig. 3; supplementary material Fig. S3 and Table S1), we found no significant difference between the Wg amplitudes in wild-type compartments and those that overexpressed the receptor. If the staining revealed the total amount of Wg, then the analytical model (supplementary material Fig. S2 and supplementary methods) suggests that the majority of Wg is not receptor bound.

A simplified analytical model predicts narrowing of Wg distribution upon receptor overexpression

Assuming further that Wg decay occurs only in complex with its receptors (leading to $k_{Wg}=0$), the analytical model predicts a narrowing of the Wg gradient in regions of receptor overexpression – an n-fold upregulation of the receptor would lead to a decrease in the Wg decay length (the distance from the Wg source, where the Wg concentration is reduced by a factor of 1/e from its maximal value) by a factor $1/\sqrt{(n)}$ in the receptor-overexpression (OE) region (supplementary methods). Remarkably, theory and experiment coincided within the measurement error for compartmental Arr

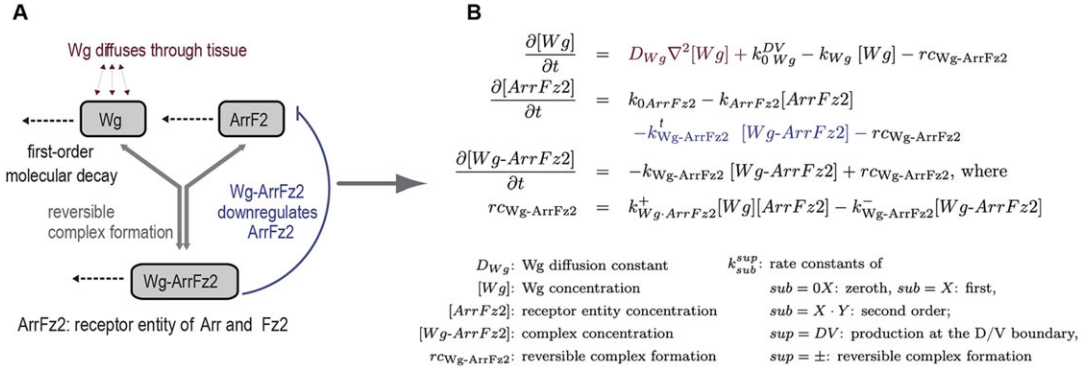

Fig. 2. Model representing Wg-induced negative regulation of Arr and Fz2. (A) Dotted arrows denote the first order decay of either single molecules or complexes of molecules; the reversible formation of complexes is denoted by groups of arrows. This mechanistic model can be translated into a set of differential equations (B).

Development (2014) 141, 2483-2493 doi:10.1242/dev.108662

overexpression experiments; we found $\lambda^{OE,Arr}/\lambda^{wt}=0.7\pm0.1$ (Fig. 3M; supplementary material Table S1), whereas the simple model predicted $\lambda_{th}^{OE,Arr}/\lambda_{th}^{wt}=1/\sqrt{n}=1/\sqrt{2}=0.7$ for the upregulation of Arr by a factor of n=2.

Receptors hinder diffusion of Wg

Extending our Wg receptor interaction model to two dimensions, we numerically solved the corresponding system of differential equations (displayed in Fig. 2) on a mesh, which resembled the cell shapes at the apical side of the wing disc. The vertex model describes cells and their contact surfaces as polygons that are composed from connected vertices with positions that are defined by the local minimum of an energy function (Farhadifar et al., 2007). Using these polygons as local control volumes, we discretized the diffusion of Wg by using the Finite Volume Method. Our modeling approach allowed us to study the consequences of changing receptor levels with cellular resolution in patches of cells, disc compartments or the entire wing pouch.

Simulating receptor overexpression in entire compartments (Fig. 4) led to a narrower Wg distribution than that in the corresponding wild-type compartments (Fig. 4B,C,F; supplementary material Table S1). These findings are also supported by our measurements of the extracellular Wg gradients (Fig. 3J-L; supplementary material Fig. S3). In our model, cells that overexpressed ArrFz2 hindered the spreading of Wg, the only diffusing protein of the model; thus, these cells serve as a 'sink' for Wg if placed next to wild-type cells (Fig. 3) – cells that overexpressed ArrFz2, positioned immediately adjacent to wild-type cells, exhibited pathway activity (simulated by the amount of Wg-ArrFz2 complex formation) further away from the Wg source than the overexpressing cells that were not adjacent to wild-type cells (Fig. 4E). In our model, these cells receive unbound Wg from neighboring wild-type cells (see Discussion).

Abrupt changes in receptor levels lead to detrimental phenotypic effects

The clonal abrupt upregulation of the receptor levels by using *tubulinα1>CD2,y⁺>arr* or *tubulinα1>CD2,y⁺>fz2* transgenes caused detrimental phenotypic defects in the wings and legs of adult flies; in wings, we detected clones that caused typical Wg gain-of-function phenotypes, such as blistering and ectopic sensory-margin

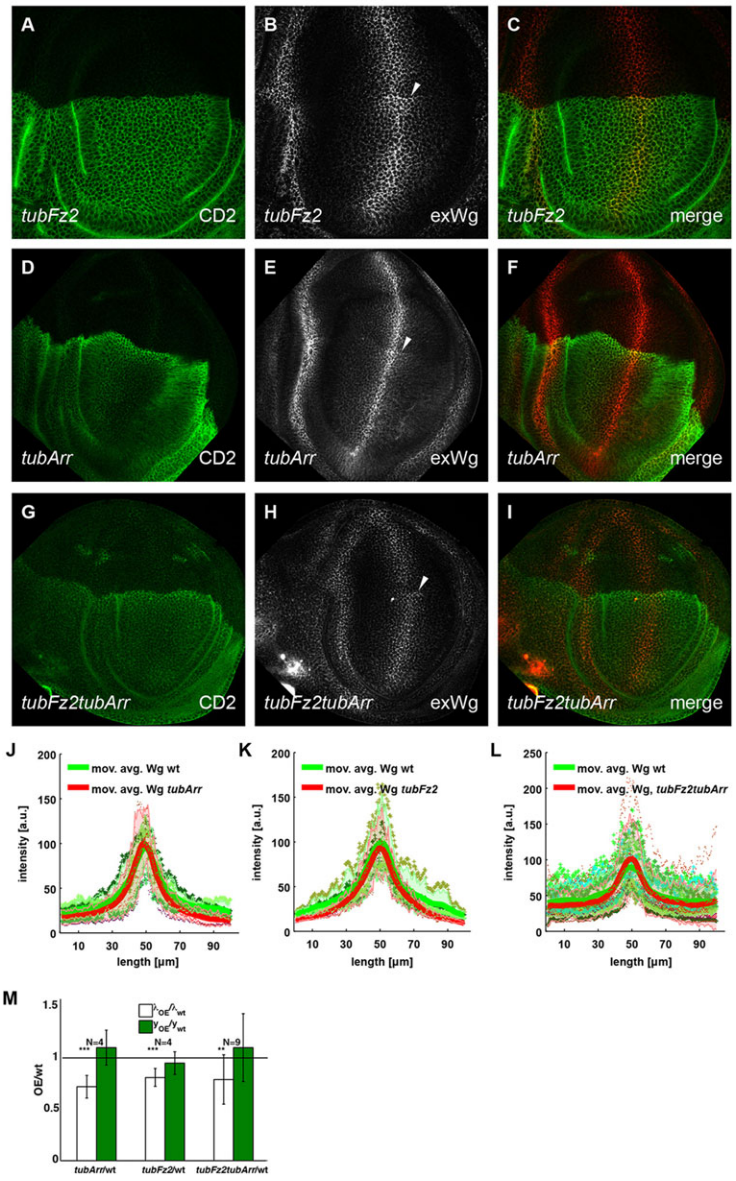

Fig. 3. Compartmental misexpression of Arr and Fz2 leads to accumulation of Wg at the edge that is shared between wild-type and receptor-overexpressing cells and to a slightly decreased distribution of Wg. The posterior (towards the top of the image) and anterior compartments of the wing imaginal discs are marked by the absence and presence of CD2, respectively. Arrowheads indicate the point of Wg accumulation. (A-C) Expression of *tubFz2* in the P compartment led to an accumulation of extracellular Wg, exactly at the boundary between the A and P compartments. (D-I) Expression of *tubArr* in the P compartment, or *tubArr* and *tubFz2* together, led to a similar extracellular Wg accumulation. (J-L) Wg level intensity plots in discs that compartmentally overexpressed Arr (J, n=4), Fz2 (K, n=4) and simultaneous overexpression of Arr and Fz2 (L, n=9), where n denotes the number of discs. Green-shaded crosses denote Wg intensities in the A compartment, red-shaded dots denote Wg intensities in the receptor-overexpressing P compartment. The moving average and standard error are defined as described in Fig. 1. a.u., arbitrary units. (M) Quantification of the change in Wg decay length (λ) and amplitude (y) upon receptor overexpression. Within each disc, we calculated the ratio between the decay length (white) and amplitude (green) in the receptor-overexpression (OE) and wild-type (wt) compartments. The bar charts display the mean and standard deviation for each experimental set up. We tested the null hypothesis, that decay length and amplitude were unchanged upon receptor overexpression, ***P<0.001, **P<0.01.

Development (2014) 141, 2483-2493 doi:10.1242/dev.108662

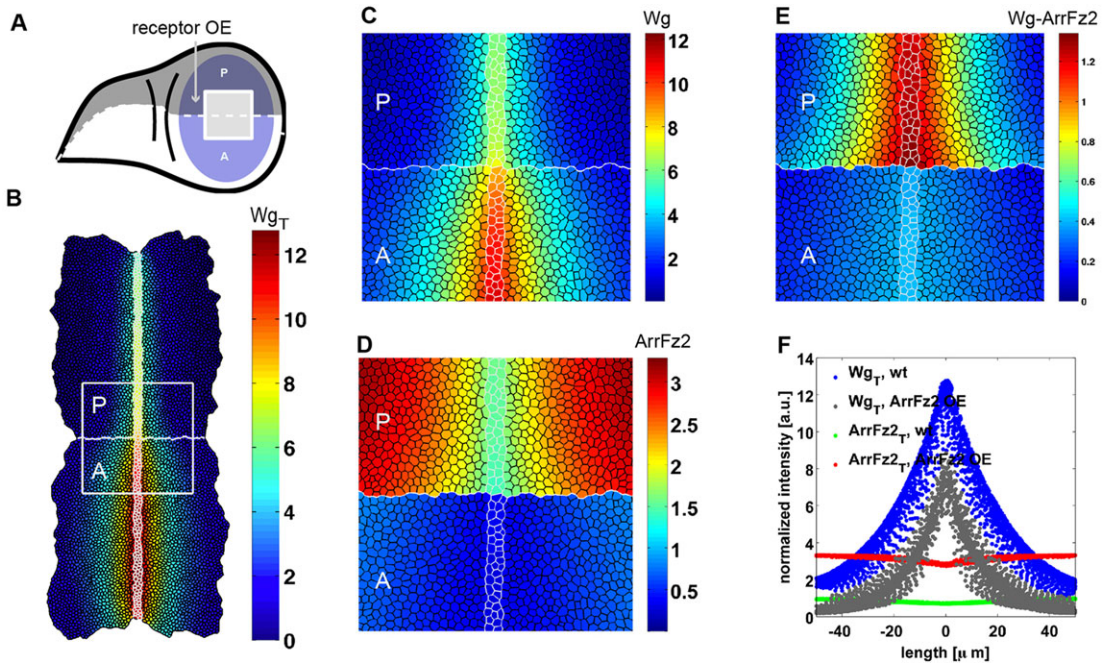

Fig. 4. Modeling reveals ectopic pathway activation in receptor-overexpressing cells juxtaposed with wild-type ells. (A) Schematic view of a wing disc. The posterior (P) compartment of the wing pouch is marked in dark blue, and the anterior (A) compartment is marked in light blue. (B) An example simulation result shows the total Wg concentration of a disc, where the ArrFz2 production rate was increased by a factor *n=3* in all cells of the upper (P) compartment. Concentrations are displayed using Matlab's jet algorithm, where red corresponds to high, and blue corresponds to low concentrations. All concentrations were normalized to the maximum value of the receptor entity ArrFz2 in wild-type discs and are given in arbitrary units. The white square corresponds to a zoomed-in region of 80 µm×80 µm centered around the intersection of the dorsal-ventral and anterior-posterior compartment boundaries. (C-E) Wg (C), ArrFz2 (D) and Wg-ArrFz2 (E) distributions of the zoomed-in region of B. Wg-expressing cells are marked by white cell edges, the anterior-posterior compartment boundary is marked by a white (horizontal) line. Note the narrowing of the total Wg distribution in the receptor-overexpressing compartment. (C) The model predicted reduced levels of diffusible Wg in anterior cells that were adjacent to the compartment boundary. (E) The distribution of Wg-ArrFz2 broadened in posterior cells that were adjacent to the compartment boundary. (F) The total ArrFz2 concentrations (defined as the sum of free and Wg-bound receptor) in a wild-type wing disc (green) and in an ArrFz2-overexpressing wing disc (red) was projected onto the anteroposterior axis. Each cell in the tissue corresponds to one dot in the graphic. Total Wg levels in a wild-type simulation are shown in blue and in an ArrFz2-overexpression simulation in gray. a.u., arbitrary units.

bristles (Fig. 5A). In legs, we found limb bifurcations that created supernumerary appendages (Fig. 5B), or an absence of tarsal segments and claws (Fig. 5C).

As an additional line of experimental validation, and to reach a higher level of reproducibility, we obtained clones that overexpressed Arr and Fz2 simultaneously through the activation of the *tubulinα1>CD2, y$^+$>fz2* and *tubulinα1>CD2,y$^+$>arr* cassettes upon a *hedgehog*-driven Flp recombinase, which was specifically expressed in the posterior compartment. They showed similar defects to the flies described above. Accordingly, when probed with an antibody against the prototypical Wg target gene *Senseless* (*Sens*), cells that co-overexpressed *tub>fz2* and *tub>arr* and were adjacent to wild-type cells displayed ectopic expression of Sens (Fig. 5D-F). We observed a similar phenotype with *tub>fz2* flp-out clones (Fig. 5G-I), but not with *tub>arr* clones (Fig. 5J-L). If we induced clones overexpressing Arr with the stronger GAL4-UAS expression system (Fig. 5M-O), again, we observed upregulation of Sens at the dorsal-ventral compartment border. Thus, we conclude that perturbations of Wg receptor levels cause ectopic pathway activity in cells with high amounts of receptor, if juxtaposed with cells that have lower levels of receptor levels.

Receptor-overexpressing cells neighboring wild-type cells act as a Wg sink

To test our model – that the receptor-overexpressing cells apposed to wild-type cells, indeed, serve as a Wg sink and benefit from this situation by increased signaling – we monitored extracellular Wg in discs that misexpressed the receptors in all posterior (P) compartment cells. Consistent with our model, such discs exhibited an accumulation of extracellular Wg, exactly at the border between wild-type anterior (A) and misexpressing P cells (arrows in Fig. 3A-I). These findings also explain the very restricted upregulation of Sens, noted above, exactly at the border between wild-type cells and cells that overexpressed the receptor.

The dual role of Fz3 – stabilization of Wg, and attenuation of Fz2 and Arr

Although Arr and Fz2 constitute the main Wg receptors, Fz3 has also been implicated in modulating the Wg response. Fz3 is expressed in the wing pouch (Sivasankaran et al., 2000) and has been proposed to serve as a negative-feedback regulator of the Wg pathway (Sato et al., 1999). Unlike Fz2 and Arr, however, the expression of Fz3 seems to be positively regulated by Wg signaling (Sivasankaran et al., 2000; Sato et al., 1999). To clarify the role of Fz3 in Wg gradient formation, we overexpressed Fz3 in the P compartment and monitored Sens levels as a read-out for Wg pathway activity. Indeed, we observed decreased Sens levels in the P territory, suggesting that overexpressed Fz3 attenuates Wg signaling (Fig. 6A-C). Consistent with this finding, Sens levels are enhanced in *fz3* mutant mitotic clones (Fig. 6D-F). We wondered whether the alterations in Sens levels in *fz3* mutant tissue, or tissue that overexpressed *fz3*, were mediated by changes in the levels of Wg, Fz2 or Arr. We first monitored extracellular Wg protein in compartments that overexpressed Fz3 and observed a notably enhanced and broadened extracellular distribution of the Wg protein (Fig. 6G-J). Interestingly, Fz2 and Arr levels were reduced in such

Development (2014) 141, 2483-2493 doi:10.1242/dev.108662

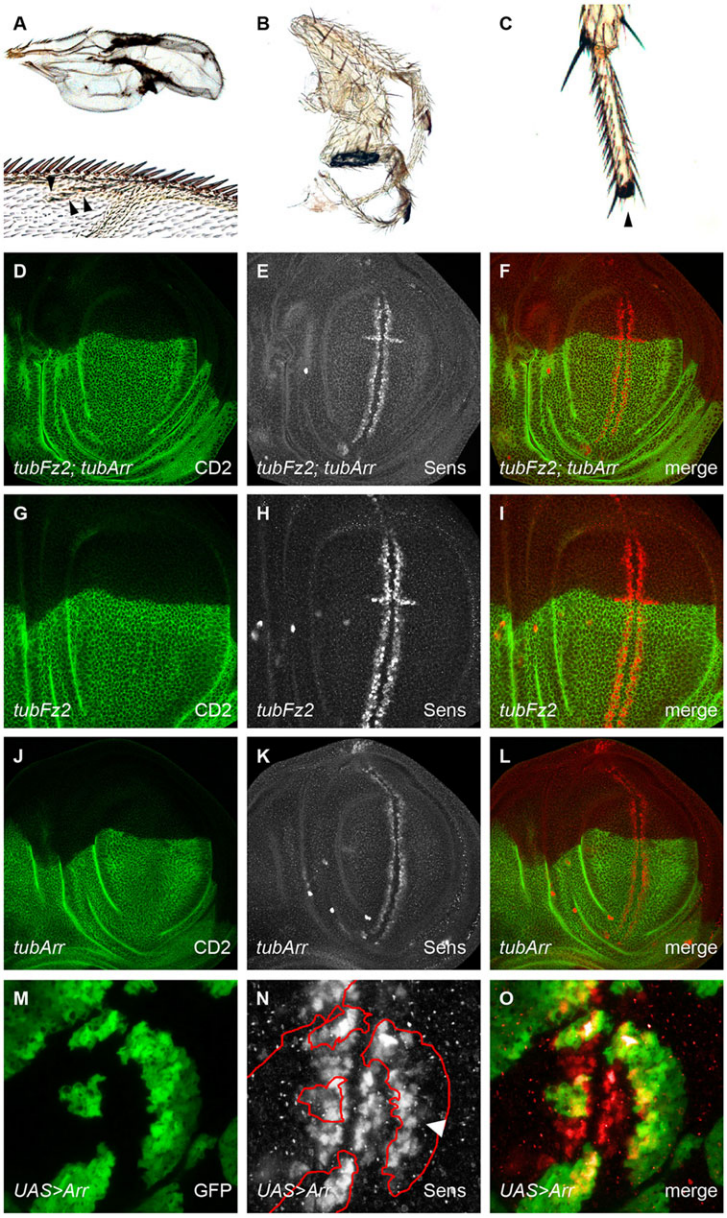

Fig. 5. Clonal overexpression of Arr and Fz2 leads to severe border effects. (A) Adult wing phenotypes that arose from random clones that expressed *tubFz2* or *tubArr* showed Wg gain-of-function defects, such as blistering and ectopic sensory bristles (arrowheads). (B,C) Random *tubFz2*- and *tubArr*-expressing mitotic clones resulted in bifurcations and truncations in legs. (D-F) Third-instar imaginal discs that contained *hhGal4, UAS-Flp, tubFz2, tubArr* clones (D-F) showed ectopic expression of the Wg target Sens (gray in E, red in F), predominantly in cells that were adjacent to wild-type neighbors at the border of the clone, close to the Wg source [*tubFz2*- and *tubArr*-expressing clones were marked by the absence of CD2 (green in D and F)]. (G-I) Similar to cells that expressed both receptor components, cells that only expressed *tubFz2* exhibited ectopic expression of Sens at the border of the clone (gray in H, red in I). CD2 expression is shown in green in G and I. (J-O) *hhGal4, UAS-Flp, tubArr* clones did not show strong Sens upregulation at the border with wild-type cells (J-L); however, in random heatshock-induced *UAS-GFP, UAS-Arr*-expressing clones (M-O), ectopic Sens expression at the border of the clone facing the Wg source was observed (arrowhead). CD2 staining is shown in green in J and L; Sens staining is marked by gray in K and N, and by red in L and O; GFP in M represents the Arr expression domain; the red outline in N marks the clone outline shown in M.

tissue (supplementary material Fig. S4A-F); however, the activity of a transcriptional *arr* reporter (ArrC19, described below and in supplementary material Fig. S7) did show a small increase in the area over which it was expressed (supplementary material Fig. S4G-I), suggesting that Fz3 post-translationally regulates the levels of Fz2 and Arr. By contrast, *fz3* mutant wing discs exhibited increased levels of Fz2 and, to a lesser extent, Arr (supplementary material Fig. S4M-N), but no discernible effect on the distribution of Wg was observed (Fig. 6K). Remarkably, we only observed the downregulation of Arr and Fz2 upon overexpression of Fz3, if the overexpressing cells included the Wg source (supplementary material Fig. S4A-F). In Fz3-overexpressing clones that were distant from the Wg source, Arr levels were higher, as we expected for a negative target, following attenuation of signaling (supplementary material Fig. S4J-L). This also suggests that downregulation of the receptor is not the primary cause for the observed attenuation of Wg signaling. We did not detect any upregulation of Fz2 levels in this situation. We conclude from these findings that the binding of Wg to Fz3 mediates the degradation of Arr and Fz2, presumably lowering receptor levels at the Wg-expressing stripe even further (supplementary material Fig. S4M-N), as well as broadening the area of Wg distribution through stabilizing the protein (Fig. 6G-J). These findings are supported by the observation that compartmental Fz3 overexpression, combined with RNA interference against Wg, reduces the downregulation of Arr in this compartment (data not shown).

To further define and rationalize the above observations, we incorporated Fz3 into our *in silico* model (supplementary material Fig. S5). We modeled Fz3 production to depend on the concentration of the Wg-ArrFz2 complex (our approximation of Wg pathway activity). Furthermore we assumed – as in the case of the receptor entity ArrFz2 – a reversible complex formation between Wg and Fz3. Our experimental data (supplementary material Fig. S4J-L) suggest that the Fz3-induced repression of Arr and Fz2 is mediated by Wg (albeit the exact mechanism still has to be investigated). Therefore, we assume in our model that Fz3 represses Arr and Fz2 expression only when Fz3 is interacting with Wg. The resulting extended set of differential equations is provided in the supplementary methods. Scanning the corresponding parameter

Development (2014) 141, 2483-2493 doi:10.1242/dev.108662

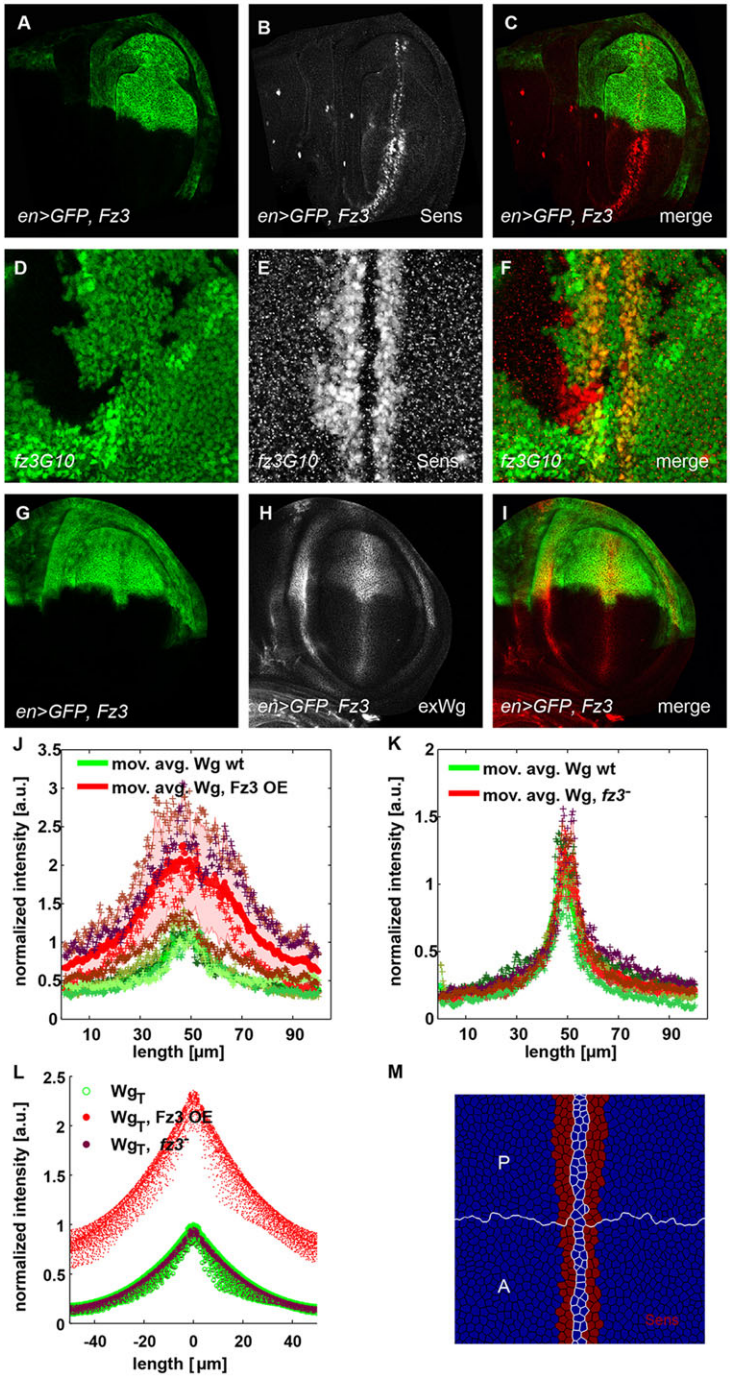

Fig. 6. Fz3 acts as an attenuator of Wg signaling.
(A-C) Overexpression of Fz3 in the P compartment (A), marked with GFP, results in a prominent reduction of Sens levels (gray in B, red in C). (D-F) Fz3 loss-of-function clones (*fz3G10*), marked by the absence of GFP (clones induced with an *FRT19, ubiGFP* chromosome) (D), led to an enhancement of Sens expression at the dorsal-ventral compartment boundary (gray in E, red in F). (G-I) Ectopic expression of Fz3 in the P compartment (G) resulted in an enhancement and broadening of the extracellular Wg gradient, revealed by immunostaining of the extracellular (ex) Wg levels (gray in H, red in I). GFP marks the P compartment. (J) Intensity profile of the Wg gradient in Fz3-overexpressing (OE) P compartments (red) and wild-type (wt) compartments (green) in a ROI of 100 μm×20 μm. *n*=8. Note the higher and broader Wg gradient in Fz3-overexpressing compartments. (K) Intensity profile of the Wg gradient in *fz3* mutant wing discs (red, $fz3^{-}$) and wild-type wing discs (green) in a ROI of 100 μm×20 μm. *n*=8. *fz3* mutant wing discs showed reduced levels of Wg and a narrower Wg distribution. (L) Results of the simulation model showed the total Wg levels (defined as the sum of free and receptor-bound Wg) in a wild-type (green), *fz3* mutant (dark red) and Fz3-overexpression simulation (light red). As in the experimental intensity profiles (J,K), Wg levels were normalized to the maximum of the wild-type expression. The simulation qualitatively reproduced the behavior of the experimental situations (J,K; supplementary material Table S1). a.u., arbitrary units. (M) A simulated profile of Senseless (red) distribution in wild-type (lower compartment) and $fz3^{-}$ cells (upper compartment). The ROI was the same as that described in Fig. 4. Wg-expressing cells are marked by white edges, and the compartment boundary is marked by a white line. We modeled Wg-expressing cells as being deficient for Senseless expression. It was assumed that all other cells with Wg-ArrFz2 concentrations higher than 95% of the maximal Wg-ArFz2 concentration expressed Senseless. A, anterior; P, posterior.

space (supplementary methods), we identified a parameter set that qualitatively reproduced the experimentally observed Wg and receptor distributions in the wild-type and receptor-misexpression conditions (the exact parameters are shown in supplementary material Table S1). Remarkably, the parameter exploration suggested that the complex that was formed by Wg and Fz3 might be more stable than the corresponding Wg-ArrFz2 complex (see supplementary material Table S2 in the supplementary methods), confirming the role of Fz3 in stabilizing Wg.

In summary, we show that Fz3 acts as an attenuator of Wg signaling in the wing pouch. We propose that Fz3 reduces the amount of Arr and Fz2 protein close to the Wg source and mediates a broader distribution of Wg.

Wg signaling indirectly represses *arr* and directly activates *fz3*

The existence of the transcriptional gradients of Arr and Fz2 prompted us to analyze by which mechanism(s) Wg signaling represses the transcription of their genes. Many feedback regulatory mechanisms of signaling pathways use direct transcriptional regulation. However, signaling-mediated transcriptional repression (as opposed to activation) has rarely been described (Affolter et al., 2008). Thus, we sought to isolate and characterize the regulatory DNA elements of *arr* and *fz2* that are responsible for the Wg input. The similar expression patterns and regulatory roles of *arr* and *fz2* led us to speculate that both genes might be transcriptionally controlled by the same molecular mechanism. Hence, we chose the *arr* locus as a case study and

Development (2014) 141, 2483-2493 doi:10.1242/dev.108662

systematically dissected its regulatory region. Seven overlapping fragments (*A* to *G*) covering 25 kb were cloned into a p*lacZ-attB* reporter vector, 5′ to an *hsp70* minimal promoter. Each construct was integrated into the same *attP* landing site on the second chromosome (Bischof et al., 2007) and the expression of lacZ in imaginal discs was analyzed. Fragment *arrC* recapitulated the endogenous *arr* expression pattern (Fig. 7A) and also properly reacted to experimentally increased and decreased Wg pathway activity, as assessed in clones that expressed *NRT-Wg* and pan^{DN}, respectively (data not shown). We next narrowed down the regulatory activity of *arrC* by using an extensive series of reporter constructs (supplementary material Fig. S7), resulting in a 200 bp fragment termed *arrC19*, which could not be shortened further without compromising activity. Clones that expressed a constitutively active version of Arm (Arm^{act}) repressed *arrC19* reporter expression, confirming that it retained the element(s) responsible for the negative Wg input (Fig. 7B-D). To check if this regulatory Wg input was mediated directly by Pan, we mutated the four highly conserved Pan binding sites in the *arrC19* enhancer. The expression pattern of the resulting *arrC19_Tcf_mut* transgene was not derepressed, suggesting that Pan is not directly involved in regulating *arrC19* (Fig. 7I). Thus, we conclude that Wg-mediated repression of *arrC19* occurs independently of the direct binding of Pan.

Furthermore, we analyzed the nature of the Wg input on *fz3* by using a similar approach – dissecting the *fz3* locus into seven overlapping fragments, *A* to *G*. The expression pattern of fragment Fz3G was the only one that was reminiscent of the pattern of *fz3*. Further dissection yielded *fz3G5*, a fragment of approximately 290 bp that retained *fz3*-like expression (Fig. 7E). Clones that expressed Arm^{act} (Fig. 7F-H) caused upregulation of *fz3G5* reporter gene activity. This regulation seems to be directly exerted by the canonical Wg pathway because it was completely abrogated upon mutation of the Pan-binding site (Fig. 7I).

We conclude that Wg signaling indirectly regulates *arr* (and presumably *fz2*), whereas *fz3* is a direct positive-target gene of the pathway. Thus, the sign of regulation by Wg of *arr* and *fz2* differs from that of *fz3* (to impact negatively and positively on their expression, respectively), as well as the mode of regulation (indirect versus direct).

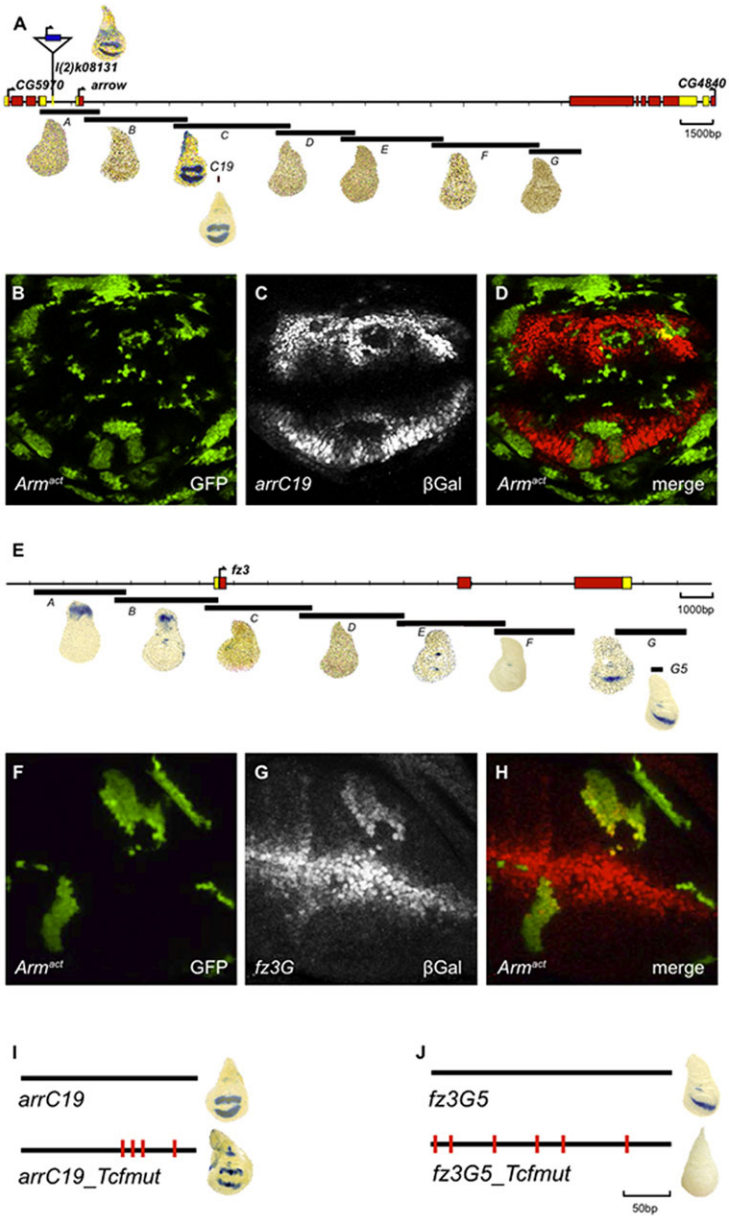

Fig. 7. *arr* is an indirect negative Wg target, and *fz3* is a direct positive Wg target. A map of the genomic region of *arr* (A). Translated exons are shown in red, untranslated regions in yellow. Fragments *A-G* were tested for their ability to activate a heterologous promoter driving *lacZ* expression (blue stain). Only fragment *C* recapitulated the *arr* expression pattern in the wing imaginal disc. Insertion of the P-element *arrZ* is shown on top. Further dissection of fragment *C* revealed the minimal enhancer fragment *arrC19* (see supplementary material Fig. S4 for further details). (B-D) Randomly induced clones that overexpressed the constitutively active *UAS-*Arm^{act}, marked with GFP in (B), led to a cell-autonomous repression of *arrC19* expression, revealed by immunostaining of β-galactosidase (gray in C, red in D) (C,D). (E) A map of the genomic *fz3* locus. Fragments *A-G* were tested for their ability to activate a heterologous promoter driving *lacZ* expression. Only fragment *G* recapitulated the *fz3* expression pattern in the wing pouch. (F-H) Overexpression of *UAS-*Arm^{act} (green) (F) results in a cell-autonomous derepression of *fz3G*, as shown by by immunostaining of β-galactosidase (gray in G, red in H) (G,H). (I) Mutation of TCF sites in conserved regions of *arrC19* did not affect the expression of the reporter. By contrast, mutation of TCF sites in the *fz3G5* reporter completely abolished reporter expression (J).

Development (2014) 141, 2483-2493 doi:10.1242/dev.108662

DISCUSSION

During the development of a metazoan organism, signaling events are precisely regulated. One frequently employed mode of regulation is feedback loops. Here, we analyzed a network of feedback loops in the *Drosophila* wing pouch that regulate receptor abundance, and thus the range of distribution and signaling output of Wg.

Receptors sequester their ligands and, thereby, impact upon the range of the signal (supplementary material Fig. S6). A transcriptional regulatory link between receptor expression and signaling activity, causing up- or downregulation of receptor levels in cells in response to the signal, can thus restrict or extend the signaling range. For example, the Hedghog (Hh) signal induces the expression of its receptor Patched (Ptc), a regulatory link which severely narrows the Hh activity gradient (Chen and Struhl, 1996). In the case of Wg, we observed the opposite – Wg signaling appeared to extend the range of Wg distribution by transcriptionally downregulating expression of *arr* and *fz2*; downregulation of the receptors hinders the formation of Wg-Arr-Fz2 complexes. This allows superfluous Wg to diffuse further away from the source without being immobilized by its receptors. In agreement with this notion, we observed a slightly narrower distribution of extracellular Wg in discs that expressed Fz2 or Arr under the *tubulinα1* promoter (Fig. 3; supplementary material Fig. S2). Quantifying these observations in discs that compartmentally overexpressed the receptor (Fig. 3; supplementary material Fig. S2 and Table S1), we observed a subtle reduction of the decay length (corresponding to a slightly steeper Wg distribution) in compartments that overexpressed the receptor compared with that in wild-type compartments.

In apparent contradiction, a previous study (Cadigan et al., 1998) has shown that high levels of Fz2 can stabilize Wg and promote Wg spreading; accordingly, we observed an accumulation of Wg when repeating this experiment by overexpressing Fz2 using the GAL4-UAS system. These contradictory findings can be reconciled by taking into account the different strength of Fz2 upregulation in the two experimental setups – Fz2 expression that is driven by the *tubulinα1* promoter leads to a relatively mild upregulation of the receptor by, approximately, a factor of 2 (Fig. 1; supplementary material Table S1), whereas overexpression by using the GAL4-UAS system causes a much stronger overexpression. Presumably, Arr becomes the limiting factor in *UAS-Fz2*-overexpressing cells, a situation that might prevent the surplus Wg-Fz2 complexes from being internalized, thus causing an extracellular accumulation of Wg (Marois et al., 2006). If Fz2 is only moderately overexpressed, sufficient Arr protein might be available to allow this extra Fz2 to form Wg-Arr-Fz2 complexes, which are subsequently internalized, leading to a slight narrowing of the gradient because there is less free and diffusible Wg. Consistent with this notion, simultaneous strong overexpression of both of the receptors Fz2 and Arr, by means of Gal4, leads to a reduction of extracellular Wg levels (Piddini et al., 2005).

Receptors act as a Wg sink

Although Wg signaling transcriptionally represses both Arr and Fz2, ubiquitous overexpression of Arr, or Fz2, had no phenotypic consequences. Unexpectedly, however, severe phenotypes arose upon mosaic expression of the *tub>arr* or *tub>fz2* transgenes. Theoretical modeling (Fig. 4) and reporter gene analysis indicated that cells that had elevated receptor levels ectopically activated the pathway when situated close to wild-type cells. Apparently, the 'high-receptor-level state' allows *tub-fz2* or *tub-arr* cells to engage in ligand-receptor interactions that depend on the 'low-receptor-level state' of their neighbors. One plausible explanation might be that *tub-fz2*, or *tub-arr*, cells bind to Wg that diffuses in from neighboring wild-type cells.

The different outcome of clonal versus uniform alteration of the Wg pathway is reminiscent of observations that have been reported by Piddini and Vincent (Piddini and Vincent, 2009), where loss of Wg signaling in the entire P compartment had no impact on the expression of low-threshold target genes but resulted in their repression, and in patterning defects, when Wg signaling was only clonally abolished. Piddini and Vincent also used different patterns of Wg receptor expression for their experiments, and they explained their findings by postulating that there is a Wg-induced, still to be identified, inhibitory signal that negatively regulates target gene expression in surrounding cells.

The negative feedback regulator Fz3

In an additional layer of negative-feedback regulation in the wing pouch, Wg signaling activates the expression of the Frizzled family member Fz3 (this work; Sato et al., 1999; Sivasankaran et al., 2000). Fz3 seems to act as a negative regulator of Wg signaling by repressing Wg signaling readouts and downregulating Wg receptor levels. Various models could be envisaged of how Fz3 acts as an inhibitor of Wg signaling. As it has been demonstrated that Fz3 is able to bind Wg (Wu and Nusse, 2002), Fz3 could work as a decoy receptor that acts as a molecular trap by binding to Wg without eliciting a signal. Decoy receptors are often part of negative-feedback mechanisms. In the *Drosophila* epidermal growth factor (EGF) system, the pathway inhibitor Argos is a target of EGF signaling and functions as a decoy receptor (Klein et al., 2004). In vertebrates, decoy Frizzled receptors have been identified that modulate Wnt signaling – secreted Frizzled-related molecules (sFRPs) have strong homology to the Frizzled extracellular domains. sFRPs inhibit signaling by directly binding to the Wnt ligands (Mii and Taira, 2011). No sFRP gene has been identified in the *Drosophila* genome.

In another scenario, Fz3 could work as a negative regulator of Wg receptors. Its function could be analogous to that of ZNRF3 and RNF43 in crypt base columnar intestinal stem cells. These related E3 ubiquitin ligases have been shown to regulate the stability and levels of cell-surface Fz and LRP5/6, through internalization and lysosomal degradation of the receptor components in the presence of Wnt signaling (Hao et al., 2012; Koo et al., 2012). Several of our experimental findings indicate that Fz3 might work as an inhibitor of Wg feedback at the receptor level – firstly, we observed decreased Arr and Fz2 levels in compartments that overexpressed Fz3 (supplementary material Fig. S2B,E), and secondly, Arr and Fz2 levels were increased in *fz3* mutant wing discs (supplementary material Fig. S4M,N). Most probably, Fz3 acts by more than one mechanism – cells that overexpressed Fz3 in the Wg stripe lead to Arr downregulation, whereas cells that overexpressed Fz3 outside of the Wg stripe lead to Arr upregulation (supplementary material Fig. S4J-L). Furthermore, extracellular Wg was stabilized upon Fz3 overexpression (Fig. 6G-I). In a wild-type situation, this stabilization of Wg might contribute to a broader Wg gradient and promote signaling in the outskirts of the wing pouch. Taken together, these findings suggest that only Wg-bound Fz3 causes inhibition of the pathway.

The role of transcriptional Wg receptor regulation

The post-translational regulation of Wg receptor levels was not the focus of this study, but we undertook substantial efforts to further characterize the transcriptional regulation of the receptor genes. In particular, we sought to identify the regulatory elements of these genes that mediated the feedback loops. The isolation of a 200 bp

Development (2014) 141, 2483-2493 doi:10.1242/dev.108662

fragment of the *arr* locus and a 300 bp fragment of the *fz3* gene – each of which was responsive to Wg signaling and drove reporter gene expression in a pattern that was reminiscent of the endogenous expression pattern – allowed us to investigate whether the Wg pathway controls these genes directly or indirectly; *fz3* appeared to be a direct target of canonical Wg signaling, whereas *arr* did not. Pan-binding sites were dispensable in the minimal *arr* enhancer, indicating that either Arm regulates the transcriptional activity of *arr* through another DNA-binding protein, or that Arm and/or Pan transcriptionally induce one (or more) negative regulators that, in turn, regulate *arr* expression. Hence, although the Wg pathway has been reported to possess the capacity to directly negatively regulate transcription (Blauwkamp et al., 2008; Affolter et al., 2008), it apparently does not use this mechanism to attenuate *arr* expression.

Including transcriptional Wg receptor downregulation in our model led to a broader distribution of Wg (supplementary material Fig. S6A) – receptor downregulation by ligand-induced endocytosis consumes the ligand, this was not the case for transcriptional repression (supplementary material Fig. S6B). The broadening of the Wg distribution area under a mechanism of transcriptional receptor repression might facilitate a robust signaling readout for high-threshold Wg target genes.

A recent study indicates that the long-range Wg gradient might be less important for imaginal disc patterning than assumed previously (Alexandre et al., 2014). Hence, it is also conceivable that the receptor gradients are not essential, a notion supported by our finding that uniform misexpression of Arr or Fz2 in the wing imaginal disc had no phenotypic consequences. Nevertheless, it remains to be determined whether the Arr and Fz2 gradients are dispensable; our *tubArr* transgene is not able to rescue *arr* loss-of-function mutants.

A cell-based ligand-receptor model

So far, most quantitative models of the Wnt-Wg pathway have focused on intracellular events (reviewed in Kofahl and Wolf, 2010), and only a few models have taken into account the spatial aspects of this signaling system (Sick et al., 2006; Ramis-Conde et al., 2008; van Leeuwen et al., 2009; Zhu, 2011). Our model is the first to systematically study the roles of Wg-receptor complexes – Wg-ArrFz2 and Wg-Fz3 – in the spatial profile of Wg signaling, as well as being the first to be challenged experimentally by manipulations of the receptor levels. Our cell-based modeling approach of ligand receptor interactions allowed us to vary all parameters in a cell-autonomous manner, which has not been done in previous studies (Eldar and Barkai, 2005; Dalessi et al., 2012; Schwank et al., 2011). This technique is, thus, an ideal tool to predict the impact of clonal conditions with cellular precision, which have historically formed the basis of experimental approaches in *Drosophila* but have also become increasingly available in vertebrates.

MATERIALS AND METHODS

Quantifying the shape of Wg and receptor distributions

We quantified the Wg intensity projections of each disc, i, by fitting an exponential decay $y_{is}=y_{0is}\times exp(-x/\lambda_{is})$, where y_{0is} is the corresponding Wg amplitude and λ_{is} the decay length, from the center of the region of interest to both sides ($s\in[left,right]$) up to 30 µm, omitting the Wg-producing source region (approximately 4 µm in width).

How well the data fitted to each curve was estimated by calculating the coefficient of determination, R^2_{is}, from the intensity projections and the fit of the curve. For the two fits, to the left and right within each region of interest (ROI), of disc number i, we calculated the mean R^2_i and the mean of the absolute values of the two decay lengths, $\lambda_i=(|\lambda_{i\,left}|+|\lambda_{i\,right}|)/2$.

We quantified the receptor intensity projections of each disc i by fitting exponential functions, linear (data not shown) and second order polynomials $y_i(x)=a_ix^2+b_ix+c_i$, where the latter showed the best overall coefficients of determination. The slope of the receptor distributions was then defined as the derivation of the second order polynomial with respect to x. Supplementary material Table S1 displays the mean fit coefficients of n measurements.

Fly stocks

Transgenic flies were generated by using the PhiC31 transgenesis system and integrated on the landing sites ZH-51D or ZH-86Fb (Bischof et al., 2007).

The following stocks were used for genetic and clonal analysis:
Sp/CyO; hhGAL4, UAS-Flp/TM6B (Pérez-Garijo et al., 2009);
yw hsp-flp; UAS-HA-NRT-Wg/SM5^; MKRS/TM6B (Zecca et al., 1996);
yw hsp-flp; UAS-ΔPan-HA/TM6B (van de Wetering et al., 1997);
yw hsp-flp; UAS-Armact (Zecca et al., 1996);
yw hsp-flp; Sp/CyO; dpp-GAL4/TM6B (Entchev et al., 2000);
yw hsp-flp; enGAL4, UAS-GFP, tubGal80ts/CyO; MKRS/TM6B (individual components are from Bloomington);
yw hsp-flp; act>CD2, y+>GAL4, UAS-GFP (Pignoni et al., 1997);
UAS-Fz3, UAS-Arr, UAS-Fz2 and UAS-PanHA (Bischof et al., 2013);
yw hsp-flp; C765-GAL4 (Nellen et al., 1996);
Tub-flp (Struhl et al., 1993);
P(lacZ) arrk08131 (Bloomington stock 665);
FRT19 (Bloomington stock 1709), *Fz3G10* (Sato et al., 1999);
fz2(c1) (Chen and Struhl, 1999);
Df(3L)fz2 (Bloomington stock 6754).

Vectors

For cloning, standard molecular biology cloning methods were used.

To generate hybrid *tubArr* and *tubFz2* constructs, the coding regions of Arr and Fz2, respectively, were cloned 3′ in-frame of the *tubulinα1* promoter and a *FRT*-flanked *>CD2,y*$^+$*>* flp-out cassette in a plasmid that contained the *tubulinα1* 3′UTR and an *attB* site for phage-mediated transgenesis.

To generate *lacZ* reporter constructs, fragments of the genomic *arr* and the *fz3* locus were amplified from *yw* genomic DNA by using PCR with primers that harbored suitable restriction enzymes for subsequent cloning into p*lacZattB*. A detailed list of the primers and constructs that were used is available upon request.

The sequences of *arrC19* and *fz3G5* containing mutated TCF sites (mutated from ttt to ccc, the site is in bold) were synthesized by Entelechon GmbH as follows: arrC19, 5′-CCAACAGCCAGCAGTCTCCCCGTT-CGACGAATTGCTAATTTATTTCACTCTTGTACCTCGGAACACGCT-TCCTATCTAGACGTTG**GAAAgggA**CCAATTTAAAGTTTATTTATGG-**CgggTATTAgggTATA**CCCTCTCTATATTTGGCATTTTTCCTGTTGC-TCTTTTTTTTTTTGCCTTTTGCAGCTGCCTCTTCGACTGGCGTTTG-TCAA**TgggTAAC**CTGTTGTGCATACTAATTTG-3′; fz3G5, 5′;-GGTAC-CCTTTCCCTGCTCTCTGGAT**GgggGGGC**TGCGTCAGAACACGGG-TAATTGGTATCAACCGAGGCACAATTA**AgggGATT**GAAGCTGCC-ACACCGCATGCCGCTCCAACGAACAACGAATCCATC**CTACcccT**T-GCCGGCCGTCGTGGCAGGCAACAAG**CCGcccc**CACTGCGGCAACA-TCGGCACAATAGCAACAGCAACTGTGCAGCAAGCGTGCAATTA-ACTCTTGTGCGCCAA**GATCcccG**CGATTAATGCGGCCCCAAGTT-CCCAGACGAAGGGACTCTAGA-3′.

Clone induction

tubArr- and *tubFz2*-expressing clones were generated by heat-shocking the larvae for 1 h at 37°C 72 h (±12 h) after egg-laying and dissected 2-3 days after clone induction. P compartments that expressed UAS constructs were generated by shifting the crosses to 29°C for 2-3 days before dissection. *NRT-Wg*-expressing clones were induced 4 days after egg-laying for 15 min at 37°C.

Immunohistochemistry

Immunostainings were performed using standard protocols. Images were taken by using a Zeiss LSM710 confocal microscope using 40× and 63× oil objectives and analyzed with the ImageJ software. Maximum z projections

Development (2014) 141, 2483-2493 doi:10.1242/dev.108662

of ROI were performed for the individual micrographs: Discs were oriented and processed in Adobe Photoshop, intensities were projected on the longer axis of the ROI, perpendicular to the dorsal-ventral compartment boundary. For each condition, we measured at least four independent discs.

The following antibodies were used against the indicated proteins: β-galactosidase (mouse, 1:2000, Promega); Arrow (rabbit, 1:15,000, a generous gift from Steve DiNardo, University of Pennsylvania, USA; Senseless (guinea pig, 1:800, a generous gift from Hugo Bellen, Baylor College of Medicine, Houston, TX, USA; Wg [mouse, 1:3 (for extracellular stainings, see Baeg et al., 2001), Developmental Studies Hybridoma Bank]; Fz2 (mouse, 1:30, Developmental Studies Hybridoma Bank); CD2 (rat, Alexa Fluor 488-conjugated, 1:25, Serotec); HA (rabbit, 1:200, Santa Cruz Biotechnology).

To detect β-galactosidase activity of the *arr* reporters, third-instar larvae were subjected to standard X-Gal reactions. For color detection, we used standard conditions.

The secondary antibodies used were Alexa Fluor 594-conjugated goat against mouse IgG, Alexa Fluor 488-conjugated goat against mouse IgG, Alexa Fluor 594-conjugated against rabbit IgG, Alexa Fluor 488-conjugated against rabbit IgG, Alexa Fluor 568-conjugated against guinea pig IgG. All were obtained from Molecular Probes and were used 1:400.

Acknowledgements

We thank S. DiNardo and H. Bellen for antibodies; G. Morata, G. Struhl and T. Kojima for fly stocks; F. Meyer and P. Herr for help with injections; and G. Hausmann, T. Valenta, M. Hödl and C. Cantù for critically reading the manuscript.

Competing interests

The authors declare no competing financial interests.

Author contributions

All authors developed the presented concepts and prepared the manuscript. S. Steiner and D.Z. performed the experiments; S. Schilling, S. Steiner and D.Z. performed the data analysis. S. Schilling developed the *in silico* model of Wg receptor interactions and wrote the supplementary methods.

Funding

The European Research Council, the Swiss National Science Foundation and the Canton of Zurich supported this work.

Supplementary material

Supplementary material available online at
http://dev.biologists.org/lookup/suppl/doi:10.1242/dev.108662/-/DC1

References

Affolter, M., Pyrowolakis, G., Weiss, A. and Basler, K. (2008). Signal-induced repression: the exception or the rule in developmental signaling? *Dev. Cell* **15**, 11-22.

Alexandre, C., Baena-Lopez, A. and Vincent, J.-P. (2014). Patterning and growth control by membrane-tethered Wingless. *Nature* **505**, 180-185.

Baeg, G. H., Lin, X., Khare, N., Baumgartner, S. and Perrimon, N. (2001). Heparan sulfate proteoglycans are critical for the organization of the extracellular distribution of Wingless. *Development* **128**, 87-94.

Baeg, G.-H., Selva, E. M., Goodman, R. M., Dasgupta, R. and Perrimon, N. (2004). The Wingless morphogen gradient is established by the cooperative action of Frizzled and Heparan Sulfate Proteoglycan receptors. *Dev. Biol.* **276**, 89-100.

Bischof, J., Maeda, R. K., Hediger, M., Karch, F. and Basler, K. (2007). An optimized transgenesis system for Drosophila using germ-line-specific phiC31 integrases. *Proc. Natl. Acad. Sci. U.S.A.* **104**, 3312-3317.

Bischof, J., Björklund, M., Furger, E., Schertel, C., Taipale, J. and Basler, K. (2013). A versatile platform for creating a comprehensive UAS-ORFeome library in Drosophila. *Development* **140**, 2434-2442.

Blauwkamp, T. A., Chang, M. V. and Cadigan, K. M. (2008). Novel TCF-binding sites specify transcriptional repression by Wnt signalling. *EMBO J.* **27**, 1436-1446.

Cadigan, K. M., Fish, M. P., Rulifson, E. J. and Nusse, R. (1998). Wingless repression of Drosophila frizzled 2 expression shapes the wingless morphogen gradient in the wing. *Cell* **93**, 767-777.

Chen, Y. and Struhl, G. (1996). Dual roles for patched in sequestering and transducing hedgehog. *Cell* **87**, 553-563.

Chen, C. M. and Struhl, G. (1999). Wingless transduction by the Frizzled and Frizzled2 proteins of Drosophila. *Development* **126**, 5441-5452.

Clevers, H. (2006). Wnt/β-catenin signaling in development and disease. *Cell* **127**, 469-480.

Dalessi, S., Neves, A. and Bergmann, S. (2012). Modeling morphogen gradient formation from arbitrary realistically shaped sources. *J. Theor. Biol.* **294**, 130-138.

Eldar, A. and Barkai, N. (2005). Interpreting clone-mediated perturbations of morphogen profiles. *Dev. Biol.* **278**, 203-207.

Entchev, E. V., Schwabedissen, A. and González-Gaitán, M. (2000). Gradient formation of the TGF-beta homolog Dpp. *Cell* **103**, 981-991.

Farhadifar, R., Roper, J.-C., Aigouy, B., Eaton, S. and Julicher, F. (2007). The influence of cell mechanics, cell-cell interactions, and proliferation on epithelial packing. *Curr. Biol.* **17**, 2095-2104.

Hao, H.-X., Xie, Y., Zhang, Y., Charlat, O., Oster, E., Avello, M., Lei, H., Mickanin, C., Liu, D., Ruffner, H. et al. (2012). ZNRF3 promotes Wnt receptor turnover in an R-spondin-sensitive manner. *Nature* **485**, 195-200.

Klein, D. E., Nappi, V. M., Reeves, G. T., Shvartsman, S. Y. and Lemmon, M. A. (2004). Argos inhibits epidermal growth factor receptor signalling by ligand sequestration. *Nature* **430**, 1040-1044.

Kofahl, B. and Wolf, J. (2010). Mathematical modelling of Wnt/β-catenin signalling. *Biochem. Soc. Trans.* **38**, 1281-1285.

Koo, B.-K., Spit, M., Jordens, I., Low, T. Y., Stange, D. E., van de Wetering, M., van Es, J. H., Mohammed, S., Heck, A. J. R., Maurice, M. M. et al. (2012). Tumour suppressor RNF43 is a stem-cell E3 ligase that induces endocytosis of Wnt receptors. *Nature* **488**, 665-669.

Marois, E., Mahmoud, A. and Eaton, S. (2006). The endocytic pathway and formation of the Wingless morphogen gradient. *Development* **133**, 307-317.

Mii, Y. and Taira, M. (2011). Secreted Wnt "inhibitors" are not just inhibitors: regulation of extracellular Wnt by secreted Frizzled-related proteins. *Dev. Growth Differ.* **53**, 911-923.

Mosimann, C., Hausmann, G. and Basler, K. (2009). [beta]-Catenin hits chromatin: regulation of Wnt target gene activation. *Nat. Rev. Mol. Cell Biol.* **10**, 276-286.

Nellen, D., Burke, R., Struhl, G. and Basler, K. (1996). Direct and long-range action of a DPP morphogen gradient. *Cell* **85**, 357-368.

Neumann, C. J. and Cohen, S. M. (1997). Long-range action of Wingless organizes the dorsal-ventral axis of the Drosophila wing. *Development* **124**, 871-880.

Pérez-Garijo, A., Shlevkov, E. and Morata, G. (2009). The role of Dpp and Wg in compensatory proliferation and in the formation of hyperplastic overgrowths caused by apoptotic cells in the Drosophila wing disc. *Development* **136**, 1169-1177.

Piddini, E. and Vincent, J.-P. (2009). Interpretation of the wingless gradient requires signaling-induced self-inhibition. *Cell* **136**, 296-307.

Piddini, E., Marshall, F., Dubois, L., Hirst, E. and Vincent, J.-P. (2005). Arrow (LRP6) and Frizzled2 cooperate to degrade Wingless in Drosophila imaginal discs. *Development* **132**, 5479-5489.

Pignoni, F. and Zipursky, S. L. (1997). Induction of Drosophila eye development by decapentaplegic. *Development* **124**, 271-278.

Ramis-Conde, I., Drasdo, D., Anderson, A. R. A. and Chaplain, M. A. J. (2008). Modeling the influence of the e-cadherin-β-catenin pathway in cancer cell invasion: a multiscale approach. *Biophys. J.* **95**, 155-165.

Rives, A. F., Rochlin, K. M., Wehrli, M., Schwartz, S. L. and DiNardo, S. (2006). Endocytic trafficking of Wingless and its receptors, Arrow and DFrizzled-2, in the Drosophila wing. *Dev. Biol.* **293**, 268-283.

Sato, A., Kojima, T., Ui-Tei, K., Miyata, Y. and Saigo, K. (1999). Dfrizzled-3, a new Drosophila Wnt receptor, acting as an attenuator of Wingless signaling in wingless hypomorphic mutants. *Development* **126**, 4421-4430.

Schwank, G., Dalessi, S., Yang, S.-F., Yagi, R., de Lachapelle, A. M., Affolter, M., Bergmann, S. and Basler, K. (2011). Formation of the long range Dpp morphogen gradient. *PLoS Biol.* **9**, e1001111.

Sick, S., Reinker, S., Timmer, J. and Schlake, T. (2006). WNT and DKK determine hair follicle spacing through a reaction-diffusion mechanism. *Science* **314**, 1447-1450.

Sivasankaran, R., Calleja, M., Morata, G. and Basler, K. (2000). The Wingless target gene Dfz3 encodes a new member of the Drosophila Frizzled family. *Mech. Dev.* **91**, 427-431.

Struhl, G., Fitzgerald, K. and Greenwald, I. (1993). Intrinsic activity of the lin-12 and Notch intracellular domains in vivo. *Cell* **74**, 331-345.

van de Wetering, M., Cavallo, R., Dooijes, D., van Beest, M., van Es, J., Loureiro, J., Ypma, A., Hursh, D., Jones, T., Bejsovec, A. et al. (1997). Armadillo coactivates transcription driven by the product of the Drosophila segment polarity gene dTCF. *Cell* **88**, 789-799.

van Leeuwen, I. M. M., Mirams, G. R., Walter, A., Fletcher, A., Murray, P., Osborne, J., Varma, S., Young, S. J., Cooper, J., Doyle, B. et al. (2009). An integrative computational model for intestinal tissue renewal. *Cell Prolif.* **42**, 617-636.

Wehrli, M., Dougan, S. T., Caldwell, K., O'Keefe, L., Schwartz, S., Vaizel-Ohayon, D., Schejter, E., Tomlinson, A. and DiNardo, S. (2000). arrow encodes an LDL-receptor-related protein essential for Wingless signalling. *Nature* **407**, 527-530.

Wu, C.-h. and Nusse, R. (2002). Ligand receptor interactions in the Wnt signaling pathway in Drosophila. *J. Biol. Chem.* **277**, 41762-41769.

Zecca, M., Basler, K. and Struhl, G. (1996). Direct and long-range action of a Wingless morphogen gradient. *Cell* **87**, 833-844.

Zhu, H. (2011). Spatiotemporally modulated Vestigial gradient by Wingless signaling adaptively regulates cell division for precise wing size control. *J. Theor. Biol.* **268**, 131-140.

Supplementary methods

The supplementary methods explains in detail our strategy to explore the parameter space of the Wg receptor interactions based on the observed shapes of decay lengths and amplitudes.

Supplementary methods

Schilling et al.:
A regulatory network of receptors directs range and output of the Wingless morphogen

1 Differential equations describing the Wg-receptor interactions

Our extended model of Wg receptor interactions (sketched in Fig. S5) includes, besides the receptors Arr and Fz2 (summarized in the entity ArrFz2) already present in the core model (Fig. 2), the additional receptor Fz3. Thus the full set of differential equations describing the interaction of Wg with its receptors Arr, Fz2 and Fz3 is given by:

$$\frac{\partial [Wg]}{\partial t} = D_{Wg}\nabla^2[Wg] + k_{0\,Wg}^{DV}(\vec{x}) - k_{Wg}\,[Wg] - rc_{Wg\text{-}ArrFz2} - rc_{Wg\text{-}Fz3}, \tag{S.1}$$

$$\frac{\partial [ArrFz2]}{\partial t} = p_{ArrFz2}^{OE}\cdot k_{0\;ArrFz2} - d_{ArrFz2}^{OE}\cdot k_{Wg\text{-}ArrFz2}^{t}[Wg\text{-}ArrFz2] - k_{ArrFz2}[ArrFz2] - rc_{Wg\text{-}ArrFz2} - k_{Wg\text{-}Fz3\cdot ArrFz2}[Wg\text{-}Fz3][ArrFz2], \tag{S.2}$$

$$\frac{\partial [Wg\text{-}ArrFz2]}{\partial t} = -k_{Wg\text{-}ArrFz2}\,[Wg\text{-}ArrFz2] + rc_{Wg\text{-}ArrFz2} - k_{Fz3\cdot Wg\text{-}ArrFz2}[Fz3][Wg\text{-}ArrFz2], \tag{S.3}$$

$$\frac{\partial [Fz3]}{\partial t} = k_{Fz3}^{pr}[Wg\text{-}ArrFz2] - k_{Fz3}[Fz3] - rc_{Wg\text{-}Fz3} + k_{0\,Fz3}^{OE}, \tag{S.4}$$

$$\frac{\partial [Wg\text{-}Fz3]}{\partial t} = -k_{Wg\text{-}Fz3}\,[Wg\text{-}Fz3] + rc_{Wg\text{-}Fz3}, \tag{S.5}$$

where the reversible complex formation of the ligand Wg (denoted by L) with its receptors $R_1 = ArrFz2$ or $R_2 = Fz3$ is denoted by

$$rc_{L\text{-}R_i} = k_{L\cdot R_i}^{+}[L][R_i] - k_{L\text{-}R_i}^{-}[L\text{-}R_i] \tag{S.6}$$

for $i \in [1, 2]$.
The law of mass conservation implies that ligand and receptor concentration are related by

$$[Wg_T] = [Wg] + [Wg\text{-}ArrFz2] + [Wg\text{-}Fz3], \tag{S.7}$$

$$[ArrFz2_T] = [Wg\text{-}ArrFz2] + [ArrFz2], \tag{S.8}$$

$$[Fz3_T] = [Wg\text{-}Fz3] + [Fz3], \tag{S.9}$$

where the subscript T denotes the total concentration of ligand and receptors.

2 Simplifications

2.1 Neglecting Fz3

The Wg distribution in $fz3^-$ mutant discs is very similar to the corresponding wild-type distribution (Table S1). This observation suggests, that in the wild-type situation Fz3 has only a minor impact on the shaping of the Wg gradient. In a first parameter scan, we therefore reduced the number of free parameters by setting the Fz3 production rate, k_{Fz3}^{pr}, to zero. The equation system eq. (S.1-S.5) simplifies then to

$$\frac{\partial[Wg]}{\partial t} = D_{Wg}\nabla^2[Wg] + k_{0\,Wg}^{DV}(\vec{x}) - k_{Wg}\,[Wg] - rc_{Wg\text{-}ArrFz2}, \tag{S.10}$$

$$\frac{\partial[ArrFz2]}{\partial t} = p_{ArrFz2}^{OE}\cdot k_{0\;ArrFz2} - d_{ArrFz2}^{OE}.k_{Wg\text{-}ArrFz2}^{t}[Wg\text{-}ArrFz2] - k_{ArrFz2}[ArrFz2] - rc_{Wg\text{-}ArrFz2}, \tag{S.11}$$

$$\frac{\partial[Wg\text{-}ArrFz2]}{\partial t} = -k_{Wg\text{-}ArrFz2}\,[Wg\text{-}ArrFz2] + rc_{Wg\text{-}ArrFz2} \tag{S.12}$$

and the mass balance simplifies to

$$[Wg_T] = [Wg] + [Wg\text{-}ArrFz2], \tag{S.13}$$

$$[ArrFz2_T] = [Wg\text{-}ArrFz2] + [ArrFz2]. \tag{S.14}$$

The above equation system describes the Wg-ArrFz2 interactions schematically presented in Fig. 2 of the main text.

2.2 Constant receptor levels in discs lacking endogenous Fz2

In discs lacking all endogenous Fz2, but expressing a $tubFz2$ construct ($fz2^{-}tubFz2$ discs), Wg-induced Fz2 downregulation is purely post-transcriptional.

Remarkably, such discs showed only a very weak Fz2 gradient over the entire disc (Fig. S1). This finding indicates, that the post-transcriptional receptor downregulation seems to have only a small impact on the receptor gradient formation.

This low impact (leading to a nearly constant receptor distribution) might be explained by an excess of unbound receptor compared to the Wg complex: If $[ArrFz2] >> [Wg\text{-}ArrFz2]$ (caused by either an excess of receptor or a high dissociation constant of the receptor complex), then only a small receptor fraction would be post-transcriptionally regulated by Wg binding, subsequent internalization and decay.

Based on our findings in $fz2^{-}tubFz2$ discs, we will therefore make the following simplifications to study the role of receptor upregulation on Wg gradient formation:

$$[R_1] \approx [R_1]_T \equiv [R_1]_{T,0} = const, \qquad k_{L\text{-}R_1}^{t} = 0 \tag{S.15}$$

where we introduced the shorter notation

$$L \equiv Wg,\ R_1 \equiv ArrFz2.$$

Under the assumption of constant receptor levels, we obtain from eq. (S.12) in steady state

$$[L\text{-}R_1] = \frac{1}{k_{L\text{-}R_1}} rc_{L\text{-}R_1} = \frac{1}{k_{L\text{-}R_1}}\left(k_{L\cdot R_1}^{+}[L]\cdot[R_1]_{T,0} - k_{L\text{-}R_1}^{-}[L\text{-}R_1]\right). \tag{S.16}$$

Solving eq. (S.16) for $[L\text{-}R_1]$ we then obtain a linear relationship between receptor-bound (and thus not diffusing) and diffusing Wg:

$$[L\text{-}R_1] = \frac{k_{L\cdot R_1}^{+}[R_1]_{T,0}}{k_{L\text{-}R_1}^{-}+k_{L\text{-}R_1}}[L] = \frac{1}{k_{L\text{-}R_1}}\alpha_e^{L\text{-}R_1}[L], \tag{S.17}$$

where we introduced the effective complex-induced degradation rate

$$\alpha_e^{L\text{-}R_1} = k_{L\text{-}R_1} \frac{k^+_{L\cdot R_1}[R_1]_{T,0}}{k^-_{L\text{-}R_1}+k_{L\text{-}R_1}}. \tag{S.18}$$

Note that $\alpha_e^{L\text{-}R_1}$ does not only depend on kinetic constants, but also linearly on the total mount of receptor. Eq. (S.10) reduces in steady state to

$$k_0^{DV}{}_L(\vec{x}) = -D_L\nabla^2[L](\vec{x}) + k_{Wg}[L] + rc_{L\text{-}R_1}. \tag{S.19}$$

From eq. (S.16-S.17) we obtain

$$rc_{L\text{-}R_1} = \alpha_e^{L\text{-}R_1} \cdot [L], \tag{S.20}$$

which allows us to uncouple eq. (S.19) from the Wg-receptor complex concentration:

$$k_0^{DV}{}_L(\vec{x}) = -D_L\nabla^2[L](\vec{x}) + \alpha_e[L](\vec{x}), \tag{S.21}$$

where

$$\alpha_e = \alpha_e^{L\text{-}R_1} + k_L. \tag{S.22}$$

Eq. (S.21) is a a second order ordinary differential equation (ODE) describing the diffusion of the free ligand Wg (with diffusion constant D_{Wg}) and an "effective degradation rate" α_e, which summarizes the degradation of external, free Wg due to its binding to its receptor, $\alpha_{L\text{-}R_1}$, and its irreversible decay, k_{Wg}.

2.3 One dimensional analytical solution in steady state

With the simplifications (no Fz3,constant receptor levels, no transcriptional receptor regulation) introduced in the previous section, we can find an analytical, one dimensional solution of the Wg distribution (eq. (S.21)).

We consider a constant ligand production in an extended region $[-x_0, 0]$,

$$k_0^{DV}(x) = \frac{s_0}{x_0}\Theta(-x)\Theta(x+x_0). \tag{S.23}$$

Then the Wg distribution outside the production region is given by (Schwank et al., 2011))

$$\begin{aligned} L(x < x_0) &= -f^+(x) \\ L(x > 0) &= -f^-(x), \end{aligned} \tag{S.24}$$

where we defined

$$\begin{aligned} f^\kappa = \frac{s_0}{2x_0\alpha_e}(1 - e^{\kappa x 0/\lambda}) \quad (e^{\kappa x/\lambda}) \\ = C_0 \quad (e^{\kappa x/\lambda}) \end{aligned} \tag{S.25}$$

with $\kappa \in [+,-]$ and the decay length

$$\lambda_e = \sqrt{D/\alpha_e}, \tag{S.26}$$

where α_e is the effective decay rate of the free (external) Wg contribution and λ_e is the corresponding effective decay length. The decay length λ_e corresponds to the distance at which the concentration is reduced by a factor 1/e of C_0. As eq. (S.25) is a purely exponential decay with decay length λ_e, the width of the source, x_0, only impacts the amplitude C_0 of the ligand distribution.

Inside the production region we have

$$L(x \in [-x_0, 0]) = \frac{s_0}{2x_0\alpha_e}(2 - e^{x/\lambda} - e^{-(x+x_0)/\lambda}) \tag{S.27}$$

leading to a flattened ligand profile (Schwank et al., 2011).

3 Relative abundance of free and receptor-bound ligand

The relative abundance of free and receptor-bound ligand Wg over the whole (one dimensional) tissue is given for each component $I_\beta = \int dx \beta(x)$ with $\beta \in [L, L\text{-}R_1]$ by

$$a \equiv I_L = \frac{s_0}{\alpha_e}, \qquad (1-a) \equiv I_{L\text{-}R_1}, \tag{S.28}$$

where we have introduced the fraction of unbound ligand $a \in]0,1[$ and the global concentration normalization

$$I_{L_T} = I_L + I_{L\text{-}R_1} = 1. \tag{S.29}$$

From eq. (S.18) follows then for the receptor-bound Wg fraction

$$I_{L\text{-}R_1} = (1-a) = \frac{\alpha_e^{L\text{-}R_1}}{\alpha_e} \frac{s_0}{k_{L\text{-}R_1}} = a \cdot \frac{\alpha_e^{L\text{-}R_1}}{k_{L\text{-}R_1}}. \tag{S.30}$$

The above equation leads to the following relation between the effective receptor complex decay and the irreversible complex decay rate:

$$\frac{I_{L\text{-}R_1}}{I_L} = \frac{1-a}{a} = \frac{\alpha_e^{L\text{-}R_1}}{k_{L\text{-}R_1}}, \tag{S.31}$$

which leads to

$$k_{L\text{-}R_1} = \frac{a}{1-a} \alpha_e^{L\text{-}R_1}. \tag{S.32}$$

The relative amount of unbound ligand is thus defined by the irreversible decay of the complex and the effective diffusion constant of free Wg:

$$a = \frac{k_{L\text{-}R_1}}{\alpha_e^{L\text{-}R_1} + k_{L\text{-}R_1}}. \tag{S.33}$$

In the most simple model we assume - besides constant receptor levels, no transcriptional receptor regulation and no impact of Fz3 on the Wg distribution - that the Wg decay is dominated by receptor binding and subsequent internalization ($\alpha_{L\text{-}R_1} >> k_L$). Neglecting the irreversible decay of free Wg, we obtain from eq. (S.22)

$$\alpha_e = \alpha_{e,s} = \alpha_e^{L\text{-}R_1}, \tag{S.34}$$

where the subscript "s" denotes here and in the following this most "simple" model. Under this assumption eq. (S.30) simplifies to

$$I_{L\text{-}R_1} = (1-a) = \frac{s_0}{k_{L\text{-}R_1}}. \tag{S.35}$$

Thus in the simple model, the constants α_e and $k_{L\text{-}R_1}$ are fully determined by the relative fractions of unbound and bound Wg, respectively.

For the relationship between total and unbound ligand we obtain with eqs. (S.18) and (S.31)

$$L_T = L + [L\text{-}R_1] = L + \frac{\alpha_e^{L\text{-}R_1}}{k_{L\text{-}R_1}} L = L + \frac{1-a}{a} L = \frac{L}{a}. \tag{S.36}$$

In our Wg stainings, we cannot distinguish between free and receptor-bound Wg and can thus not extract the relative fraction of unbound Wg a from the above equation. But the following section will show, that comparing the peaks of Wg expression in wild-type and receptor-overexpression regions, allows an estimation of this fraction.

4 Constraining the parameter space by comparing the Wg profile in wild-type vs. receptor-overexpressing regions

We model receptor overexpression by increasing the total amount of receptor by a factor $n = p^{OE}_{ArrFz2}$ in the receptor-overexpressing (OE) region

$$[R_1]^{OE}_T = n \cdot [R_1]_{T,0}, \tag{S.37}$$

where $[X]^{OE}$ denotes in the following the concentration of protein X in the receptor-overexpressing region $C = [x1, x2]$: $X^{OE} \equiv [X](x \in C)$. Accordingly, the absence of the superscript OE denotes the corresponding wild-type concentration in the same distance $|x|$ from the Wg source.

In the simple model an n-fold receptor upregulation leads to an n fold larger effective decay rate $\alpha_e^{OE\ L\text{-}R_1} = n\alpha_e^{L\text{-}R_1}$. Accordingly the decay length of free Wg gets reduced by a factor $1/\sqrt{n}$, as with eq. (S.17) we have

$$\lambda^{OE}_{e,s} = \sqrt{\frac{D}{\alpha^{OE\ L\text{-}R_1}}} = \sqrt{\frac{D}{n \cdot \alpha^{L\text{-}R_1}}} = \frac{1}{\sqrt{n}}\lambda_{e,s}, \tag{S.38}$$

where the subscript “s” indicates in the following this most ”simple” relation between wild-type and receptor-overexpression decay lengths.

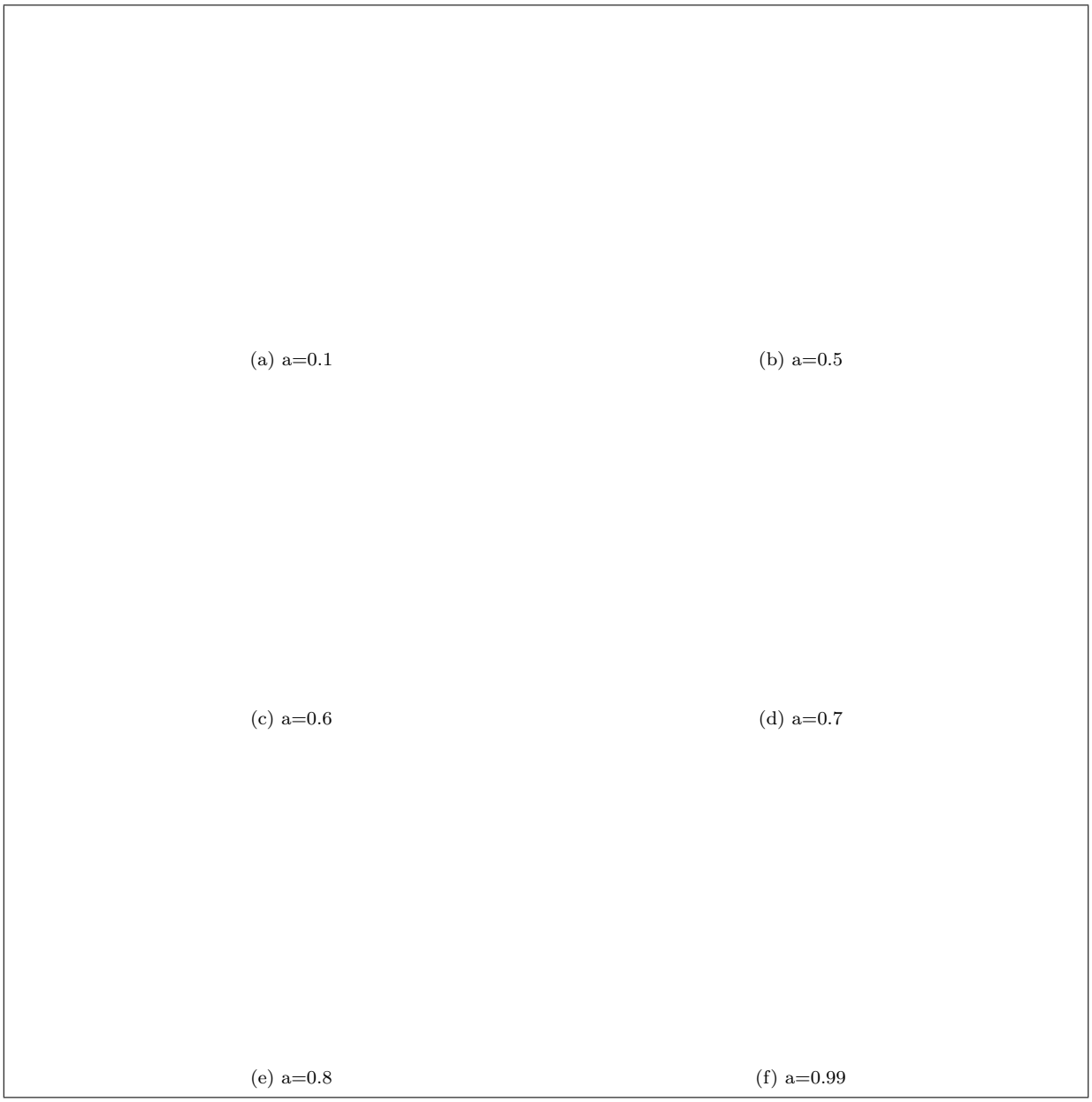

(a) a=0.1 (b) a=0.5

(c) a=0.6 (d) a=0.7

(e) a=0.8 (f) a=0.99

Figure A1: **Comparison of Wg distributions in wild-type (solid lines) and receptor-over expressing regions (x > 0) for dot-dashed lines.**
To mimic Arr overexpressing experiments, we increased the amount of receptor by a factor $n = 2$ for $x > 0$ in graphs with dot-dashed lines. We show the total amount of Wg (black), its free (red) and receptor-bound (green) components and vary the relative amount of free Wg, a. The Wg source is situated between $x_0 = -1/20\ H$ (blue dashed line) and $x = 0$. The decay length of free Wg is set to $\lambda_{Wg} = 22\ \mu$m, the average wild-type decay length measured in discs, where Arr was compartmentally overexpressed. H indicates the half width of the region of interest of length 50 μm.

In Fig. A1 we study the impact of receptor upregulation on the distributions of freely diffusing Wg (red), receptor bound Wg (green) and the total amount of Wg (black) in the simple model. In all plots with dashed lines, we upregulated the amount of receptor by a factor $n = 2$ for $x > 0$. We varied the amount of unbound ligand, a, in between the panels (a) to (f). Solid lines show the distributions in a corresponding wild-type disc. As expected from eq. (S.17), we observe in all scenarios an upregulation of Wg-$ArrFz2$ by a factor n in the overexpression region. The explicit solution for the free ligand in and outside the overexpressing region has been derived in section 4.2 of the supplement of (Schwank et al., 2011). Fig. A1 reveals the dependence of the increase of the amplitude of total Wg (black) in receptor overexpression regions on the relative amount of free ligand a: The higher a, the less the amplitude of the total Wg distribution gets affected by changes in receptor levels. In fact, Schwank et al. have shown (Schwank et al., 2011), that in the most simple model there is a (negative) linear relationship between the fold change ρ of the amplitudes in receptor-overexpressing regions and a.

Comparing the amplitudes of Wg expression in wild-type and receptor-overexpressing compartments (Table S1), we find that they coincide within the measured error bars. Experimentally we cannot distinguish between external free and receptor bound Wg. If the antibody stainings were to show only the freely diffusing Wg (red), then it is very difficult to estimate a from the stainings - wild-type and receptor-overexpression differ for all values of a at the most approx. 25 %. But if the stainings were to reveal the total amount of Wg, Fig.?A1 suggests, that most Wg is freely diffusing ($a > 0.5$): For high values of a (corresponding to a high fraction of freely diffusing, not receptor-bound Wg), wild-type and overexpressing amplitudes differ only slightly and the theoretically predicted difference in the amplitude is in the same range as the variation between biological replica. In the latter case, we can approximate the decay length of free Wg λ_e by the effective decay length λ of all Wg contributions:

$$\lambda_e \approx \lambda. \tag{S.39}$$

Table S1 reveals an agreement between the measurement error with this simple approximation for compartmental Arr overexpression experiments: we find $\lambda^{OE}_{Arr,exp}/\lambda_{Arr,exp} = 0.7 \pm 0.1$, whereas the simple model model predicts $\lambda^{OE}_{Arr,e,s}/\lambda_{Arr,e,s} = \frac{1}{\sqrt{n}} = 0.7$ for an Arr overexpression of roughly a factor $n = 2$.

But in the case of compartmental overexpression of Fz2, the simple model suggests a steeper gradient (smaller λ) in the overexpression situation than actually measured: A Fz2 upregulation of roughly a factor $n = 3.5$ (Table S1) leads to a theoretical value of $\lambda^{OE}_{Fz2,e,s}/\lambda_{Fz2,e,s} = 0.5$, whereas experimentally we find $\lambda^{OE}_{Fz2,exp}/\lambda_{Fz2,exp} = 0.8 \pm 0.1$.

In discs where both receptors Arr and Fz2 were simultaneously upregulated, we observed a similar decrease in the decay length as compared to the upregulation of only one receptor: $\lambda^{OE}_{ArrFz2,exp}/\lambda_{ArrFz,exp} = 0.8 \pm 0.2$. This finding justifies to summarize the effect of the receptors Arr and Fz2 in the entity "ArrFz2" in our modeling approach.

Dropping the assumption of vanishing k_L we obtain

$$\lambda^{OE}_e = \sqrt{\frac{D}{\alpha_e}} = \sqrt{\frac{D}{n \cdot \alpha_e^{L\text{-}R_1} + k_L}}, \tag{S.40}$$

which forecasts a smaller decrease in λ by receptor upregulation than in the naive model. The larger the ratio $k_L/\alpha_e^{L\text{-}R_1}$, the smaller is the expected influence of receptor upregulation on the steepness of the gradient.

5 Parameter estimations

5.1 Kinetic parameters from GFP-tagged Wg in Fluorescence Recovery after Photobleaching (FRAP) experiments

Kicheva et al. (Kicheva et al., 2007) extracted the diffusion constant $D_{Wg\text{-}GFP}$ and the fraction of molecules ψ, that did not recover in the the photo bleached region of interest during the experiment, from the time-dependent recovery profile of Wg-GFP. To do so, they compared a theoretical recovery curve based on on a model, which included Wg production, decay and transport, but did not explicitly take into consideration Wg receptor interactions, with the experimental curves. They varied the fitted parameters $D_{Wg\text{-}GFP}$ and ψ to obtain the best agreement between experimental and theoretical curves and reported

$$D_{Wg\text{-}GFP} = \lambda^2_{Wg\text{-}GFP} \cdot \alpha^{exp} = (0.05 \pm 0.04)\mu\text{m}^2/\text{sec}, \tag{S.41}$$

$$\psi = 0.09 \pm 0.13. \tag{S.42}$$

From the average fluoresence in the receiving territory of Wg e expressing discs they extracted a decay length of

$$\lambda_{Wg\text{-}GFP} = (6 \pm 2)\mu\text{m} \tag{S.43}$$

from which they calculated an effective decay rate of

$$\alpha^{exp} = \frac{D_{Wg\text{-}GFP}}{\lambda^2_{Wg\text{-}GFP}} = (14 \pm 10) \cdot 10^{-4}/\text{sec}. \tag{S.44}$$

In our modeling approach, we summarize the receptors Arr and Fz2 by the receptor entity "ArrFz2". To mimic the average impact of both receptors, we calculated the average wild-type and overexpression (OE) Wg decay lengths in discs, where Arr resp. Fz2 was compartmentally overexpressed (Table S1). In this extracellular Wg antibody stainings, we obtained from a total of eight discs

$$\lambda_{Wg,ArrFz2} = (22 \pm 4)\mu\text{m} \quad \text{and} \quad \lambda^{OE}_{Wg,ArrFz2} = (16 \pm 2)\mu\text{m}. \tag{S.45}$$

Note that this value is significantly larger than the effective decay length measured for GFP-tagged Wg by Kicheva et al. (Kicheva et al., 2007) (eq. S.43). The tagging of Wg by (a relatively large) GFP molecule might hinder its free diffusion, and lead to a smaller decay length of Wg-GFP than of non-tagged Wg.

An alternative explanation for the discrepancy between the decay lengths might be that the theoretical model in Kicheva et al. (Kicheva et al., 2007) did not account for the coupling of diffusion to receptor-mediated uptake and degradation in the fitting procedure of the kinetic parameters. Recently, for the case of DPP-GFP, it has been shown (Zhou et al., 2012) that neglecting this step might lead to an underestimation of extracted diffusion rates and immobile fractions

The measured reduction of the Wg decay length described in the previous subsection is furthermore a strong indicator, that Wg-receptor interactions is indeed shaping the Wg gradient and cannot be neglected in any modeling procedure. Therefore the kinetic parameters of Kicheva et al. (Kicheva et al., 2007) where only used as starting points of our parameter exploration.

5.2 Estimating the relative impact of Wg receptor interaction on gradient formation

The measured change in the decay length under receptor overexpression of Arr and Fz2 (summarized in the following as "ArrFz2"), allows us to extract the relative impact of the complex formation and

subsequent internalization and decay on the shape of the Wg gradient. With eq. (S.38) we obtain

$$0 \leq r_\lambda = \frac{\lambda^2_{Wg,ArrFz2}}{(\lambda^{OE}_{Wg,ArrFz2})^2} \approx \frac{\lambda^2_e}{(\lambda^{OE}_e)^2} = \frac{\alpha^{OE}_e}{\alpha_e} = \frac{n\alpha^{L\text{-}R_1}_e + k_L}{\alpha^{L\text{-}R_1}_e + k_L} = \frac{(n-1)\alpha^{L\text{-}R_1}_e}{\alpha^{L\text{-}R_1}_e + k_L} + 1 = \frac{(n-1)\alpha^{L\text{-}R_1}_e}{\alpha_e} + 1. \tag{S.46}$$

Fom our measurement of the ratio of Wg decay lengths in wild-type and receptor-overexpression situations (Table S1), we obtain

$$r_\lambda = \frac{\lambda^2_{Wg,ArrFz2}}{(\lambda^{OE}_{Wg,ArrFz2})^2} = 1.7 \pm 1.1$$

Assuming an average receptor upregulation of Arr and Fz2 of $n = 3$, we obtain for the relative impact of the Wg - receptor formation an the effective Wg decay constant

$$r_{L\text{-}R_1} = \frac{\alpha^{L\text{-}R_1}_e}{\alpha_e} = \frac{(r_\lambda - 1)}{(n-1)} = 0.3 \pm 0.5 \leq 1. \tag{S.47}$$

Note that for $k_L = 0$, we would expect $r_\lambda = n$ and thus $r_{L\text{-}R_1} = 1$.

5.3 Estimation of the kinetic parameters

Assuming $\alpha_e = \alpha^{exp}$, we can now estimate $\alpha_{L\text{-}R_1}$ from eq. (S.47)

$$\begin{aligned} 0 &\leq \alpha^{L\text{-}R_1}_e = (5 \pm 11) \cdot 10^{-4}/\text{sec} \\ &\leq \alpha^{exp} = (14 \pm 10) \cdot 10^{-4}/\text{sec} \end{aligned} \tag{S.48}$$

Eq. (S.48) can only be an upper bound for the relative impact of the receptor entity "ArrFz2" on the gradient formation. Dropping the assumption of constant receptor levels and taking into account the transcriptional downregulation of the receptors by Wg, $\alpha^{L\text{-}R_1}_{e,f} \equiv k_{L\text{-}R_1} \frac{k^+_{L\cdot R_1}[R_1]}{k^-_{L\text{-}R_1} + k_{L\text{-}R_1}}$ will be significantly smaller in the centre of the disc than far away from the Wg source. The estimation of $\alpha^{L\text{-}R_1}_e$ allows us now to give limits of k_L, too:

$$\begin{aligned} 0 &\leq k_L = \alpha^{exp} - \alpha^{L\text{-}R_1}_e = (9 \pm 14) \cdot 10^{-4}/\text{sec} \\ &\leq \alpha^{exp} = (14 \pm 10) \cdot 10^{-4}/\text{sec} \end{aligned} \tag{S.49}$$

The previous section suggests, that the majority of Wg is unbound. Conservatively assuming $a = 0.5$ we get from eq. (S.32)

$$\begin{aligned} 0 &\leq k_{L\text{-}R_1} = \frac{a}{1-a}\alpha^{L\text{-}R_1}_e = \alpha^{L\text{-}R_1}_e = (5 \pm 11) \cdot 10^{-4}/\text{sec} \\ &\leq \alpha^{exp} = (14 \pm 10) \cdot 10^{-4}/\text{sec} \end{aligned} \tag{S.50}$$

Wu et al (Wu and Nusse, 2002) have measured the binding between Drosophila Wnts and Frizzleds based on a reverse binding assay, in which Wnts are presented on the surface of the cell in the form of type II transmembrane proteins, i.e. with the COOH terminus outside the cells. The cells are then incubated with the ligand-binding domain of Frizzled (the cystein rich domain) tagged with alkaline phosphatase. For the binding of Wg with its receptor Fz2 they measured a dissociation constant of $K_{D\,Wg\,Fz2} = (5.44 \pm 0.26) \cdot 10^{-9}$ Mol[1]. We used this value as an approximation for the dissociation

[1]Note that the corresponding value in (Wu and Nusse, 2002) is wrongly reported as $K_{D\,Wg,\,Fz2} = (5.44 \pm 0.26) \cdot 10^{-8}$ Mol. After personal communication with the authors of (Wu and Nusse, 2002), this error should be corrected in the online version of the article.

constant of Wg hypothetical receptor entity ArrFz2. Whereas this constant was measured in a (three dimensional) biochemical assay, our simulations of Wg receptor interactions are two dimensional. Thus we had to transform between two and three dimensions through the simple expression

$$K_{D\ ArrFz2}^{(3D)} = k_{Wg\cdot ArrFz2}^{+}/k_{Wg-ArrFz2}^{-}, \tag{S.51}$$

where h is the confinement length (Wu et al., 2011). Exploring the parameter space, we varied the confinement length between 1 and 10 micrometers.

5.4 Discussion

Here, we assumed constant receptor levels over the entire disc, justified by the absence of a pronounced gradient in discs lacking endogenous Fz2. In general, this assumption does not hold anymore: the transcriptional downregulation of the receptors Arr and Fz2 by Wg lowers the total amount of receptors up to 50% in the disc center. But under the assumption that only a small Wg fraction gets actually receptor-bound ($[Wg\text{-}ArrFz2] << [Wg]_T$ corresponding to high values of a), this receptor modulation should only have a minor impact on the distribution of total Wg (Table S1).

Thus Fig. A1 suggests that, also in the more general case, most Wg is actually freely diffusing and not bound to its receptors Arr and Fz2. Our findings coincide with the experimental observation of Kicheva et al (Kicheva et al., 2007) that only $(9 \pm 1.3)\%$ of the total amount of Wg are immobile. In our modeling approach this "immobile fraction" corresponds to the receptor-bound Wg fraction.

In the simplified analytical model presented above, we ignored the role of Fz3 on shaping the Wg gradient. Therefore the estimations for the irreversible decay rates of Wg (k_L) and the receptor complex Wg-ArrFz2 ($k_{L\text{-}R_1}$) can only be seen as upper boundaries.

6 Numerical solution of the system of differential equations

6.1 Modeling receptor-misexpression experiments

Modeling loss of receptor experiments

The experimental setup of $fz2^-$ and arr^- mutant cells was modeled by setting the zeroth order production rate of the receptor entity ArrFz2 to zero. Correspondingly, $fz3^-$ mutant cells were modeled by setting the Wg induced production rate of Fz3 to zero. In the latter case the equation system eq. (S.1-S.5) reduces to the system of partial and differential equations describing the simplified network of Wg/ArrFz2 interactions depicted in Fig. 2 of the main text and given in eq. (S.10-S.14).

Modeling receptor-overexpressing experiments

Based on our experimental observation that under the regime of the *tubulin*α1 promoter the maximal receptor levels of Arr and Fz2 were enhanced by a factor 2 to4 (Fig. 1F, 1R, Table S1), we increased the production rate of the receptor entity ArrFz2 by a factor $n = 3$ in receptor-overexpressing cells.

Our analysis of receptor levels in discs, where Arr resp. Fz2 receptor levels were overexpressed (Fig. 1), revealed that in both cases the slope in receptor-overexpressing discs was slightly reduced (Fig. 1, Table S1). But in discs expressing the *tubFz2* construct, but lacking all endogenous Fz2, the Fz2 expression gradient got weakened (Fig. S1).

This experimental finding suggests, that only the wild-type fraction of the receptor gets transcriptionally downregulated, whereas post-transcriptional downregulation seems to have a minor impact on the receptor gradient formation (Fig. S1). We incorporate these experimental observations by introducing a dampening factor d_{ArrFz2}^{OE} of the Wg signaling mediated decay rate of ArrFz2 (eq. (S.2)). Whereas this

factor is assumed to equal 1 in wild-type cells, we varied it between 0 and 1 in receptor-overexpressing cells.

To take into consideration the transcriptional upregulation of Fz3 in Fz3 overexpressing discs, we introduced an additional zeroth order, thus Wg independent, Fz3 production term $k_{0\,Fz3}^{OE}$. In the wild-type simulation runs, this additional Fz3 production term was set to 0.

6.2 Modeling diffusion on a mesh generated by a vertex model

Extending our Wg receptor interaction model to two dimensions, we wanted to numerically solve the corresponding Wg diffusion equation on a mesh, which resembled the cell shapes of the apical side of a *Drosophila* wing disc. The vertex model fulfills this requirement: It describes cells and their contact surfaces as as a graph of connected vertices with positions defined by the local minimum of an energy function. This energy functions describes the mechano-elastic properties of the tissue(Farhadifar et al., 2007) characterized by the interplay of the line tension, the term of the energy function proportional to the edge length between two connected vertices, and the cell's contractility. We parametrized the relative impact of the line tension on the normalized energy function with $\overline{\Lambda} = 0.12$ and the relative impact of the contractility with $\overline{\Gamma} = 0.04$ ('case I' of (Farhadifar et al., 2007)). These parameters were chosen such, that the resulting network of polygons resembles the network topology of the apical cells of the wing disc. Using these polygons as local control volumes, we discretized the diffusion of Wg by the Finite Volume Method.

Implementing compartment boundaries

To mimic compartmental receptor overexpression experiments, we modeled the observed sharp anterio-posterior compartment boundary (Farhadifar et al., 2007) by increasing the $\overline{\Lambda}$ by a factor 2.5 for all edges shared between an anterior and posterior cell. In analogy, we implemented the increased line tension at the dorsoventral compartment boundary (Dahmann et al., 2011) by increasing the line tension term between Wg producing cells and all other cells (Dahmann et al., 2011) by the same factor.

Modeling growth

In simulation runs, which included the growth of the disc, we had to accurately compute the two-dimensional diffusion of the Wg protein on a geometry that is itself constantly changing. We achieved this by alternating the mechanical relaxation/growth computations of the cellular vertex model (Farhadifar et al., 2007) with the numerical solution of the coupled system of ordinary and partial differential equations given in eq. (S.1.-S.9) within each cell (as described in the supplement of (Schilling et al., 2011)). This modeling approach allowed us to simulate compartmental receptor overexpression experiments with cellular resolution on a cell topology which resembles an actual wing disc (Farhadifar et al., 2007). Movies 1 and 2 show the Wg resp. ArrFz2 concentrations of an exemplary simulation run of a growing wing disc.

7 Parameter exploration based on the shapes of Wg and receptor distributions

The analytical solution of the simplified one-dimensional model suggested that the majority of Wg is freely diffusing. It allowed us furthermore to define upper boundaries for the Wg and Wg-ArrFz2 decay constants based on the measured effective Wg decay constant. We approximated the dissociation constant of the complexes Wg-ArrFz2 and Wg-Fz3 by the measured dissociation constant of Wg-DFz2. In order to set the remaining parameters of the full two dimensional numerical model, we transformed the

above systems of equations into its non-dimensional form (Dillon and Othmer, 1999; Reeves et al., 2005). This procedure leads to dimensionless groups of the kinetic parameters, which we varied up to three orders of magnitude within physiological meaningful ranges. To explore the parameter space, we varied one parameter at a time, whilst fixing all remaining parameters. A total of roughly 10'000 parameter sets was scanned. A valid parameter entering eqs. (S.1-S.9) set had to qualitatively reproduce the shape of Wg and receptor distributions in the wild-type and receptor mutant situations as parameterized in Table S1. Remarkably, the parameter exploration suggested that the complex formed by Wg and Fz3 might be more stable than the corresponding Wg-ArrFz2 complex, confirming the Wg stabilizing role of Fz3. Furthermore, only relatively high Wg diffusion constants ($D = 4\ \mu\text{m/sec}^2$ in the exemplary parameter set displayed in Table S2 below), allowed us to describe our data. This value is roughly 80 times larger than the effective diffusion coefficient of GFP-tagged Wg reported by Kicheva et. al. (Kicheva et al., 2007). However, Kicheva et al. neglected an explicit modeling of the coupling of diffusion to receptor-mediated uptake in their fitting procedure, an approach that might lead to an underestimation of the extracted diffusion coefficient (section 5.1, (Zhou et al., 2012)).

Table S2: **Characteristic units, geometry and parameters of the Wg-receptor model**

	Value	Annotation	Source
Characteristic units			
length	$L = 1\mu$m	micrometer	
time	$T = 1$ h	hour	
concentration	$U = 1000$ molecules/cell		
Geometry			
l	1 μm	confinement region of length l perpendicular to cell membrane	(Wu et al., 2011), (Dustin et al., 2001)
A_{cell}	5.4 μm^2	average wing disc cell area	(Farhadifar et al., 2007)
Parameters			
Zeroth order production	$k_0 = 67.32$ U/h		
$k_{0\,Wg}^{DV}$	k_0	production at DV boundary	(Kicheva et al., 2007)
$k_{0\,ArrFz2}$	$10^{-3} \cdot k_0$	wt production rate of ArrFz2	
n	3	average receptor upregulation	Table S1
$k_{0\,ArrFz2}^{OE}$	$n \cdot 10^{-3} \cdot k_0$	OE production rate of ArrFz2	
$k_{0\,Fz3}^{OE}$	$10^{-2} \cdot k_0$	OE production rate of Fz3	
First order production	$k_1 = 2.52$/h		
k_{Fz3}^{pr}	$0.2 \cdot k_1$	Wg signaling induced Fz3 prod.	
First order decay			
k_{Wg}	k_1	Wg decay	(Kicheva et al., 2007)
k_{ArrFz2}	k_1	ArrFz2 decay	
k_{ArrFz2}^{t}	1.2 k_1	transcriptional and translational repression of ArrFz2 by Wg-ArrFz2	
d_{ArrFz2}^{OE}	1/2	dampening factor	section 6.1
$k_{ArrFz2,2}^{OE}$	$d_{ArrFz2}^{OE} \cdot k_{ArrFz2}^{t}$	Wg signaling induced repression in receptor OE cells	
k_{Fz3}	$2 \cdot k_1$		
$k_{Wg\text{-}ArrFz2}$	$0.8 \cdot k_1$		
$k_{Wg\text{-}Fz3}$	$0.2 \cdot k_1$	Wg-Fz3 is more stable than Wg-ArrFz2	
Dissociation const. (3D)			
$K_{D,Wg\text{-}DFz2}^{3D}$	$5.4 \cdot 10^{-9}$ M	$k_{Wg-DFz2}^{-}/k_{Wg-DFz2}^{+}$	(Wu and Nusse, 2002),
$K_{D,Wg\text{-}ArrFz2}^{3D}$	$5.4 \cdot 10^{-9}$ M	approximation of dissociation constant	section 5.3
Dissociation const. (2D)			
l	$l = 1\ \mu$ m	l: confinement length	
$K_{D,Wg\text{-}ArrFz2}^{2D}$	$l \cdot K_{D,Wg\text{-}ArrFz2}^{3D}$ = 3.2 molecules/μm^2 = 17.8 molecules/A_{cell} = 0.0178 U		(Wu et al., 2011)
Equilibrium const. (2D)			
$K_{Wg\text{-}ArrFz2}$	≈ 56/U	inverse of dissociation constant	
$K_{Wg\text{-}Fz3}$	≈ 56/U		
Second order decay	k2 $[1/(T \cdot U)]$		
$k_{Fz3 \cdot Wg\text{-}ArrFz2}$	$k_2 = k_1 \cdot K_{Wg\text{-}ArrFz2}$	Fz3 introduced repression of Wg-ArrFz2	
$k_{Wg\text{-}Fz3 \cdot ArrFz2}$	k_2	Wg-Fz3 introduced repression of ArrFz2	
Diffusion const.			
D_{Wg}	4 μm^2/s=14400 μm^2/h	diffusion constant of free Wg	

References

Dahmann, C., Oates, A. C. and Brand, M. (2011). Boundary formation and maintenance in tissue development. *Nature Reviews Genetics* **12**, 43–55.

Dustin, M. L., Bromley, S. K., Davis, M. M. and Zhu, C. (2001). Identification of self through two-dimensional chemistry and synapses. *Annual review of cell and developmental biology* **17**, 133–157.

Farhadifar, R., Röper, J.-C., Aigouy, B., Eaton, S. and Jülicher, F. (2007). The influence of cell mechanics, cell-cell interactions, and proliferation on epithelial packing. *Current Biology* **17**, 2095–2104.

Kicheva, A., Pantazis, P., Bollenbach, T., Kalaidzidis, Y., Bittig, T., Jülicher, F. and González-Gaitán, M. (2007). Kinetics of morphogen gradient formation. *Science (New York, NY)* **315**, 521–525.

Schilling, S., Willecke, M., Aegerter-Wilmsen, T., Cirpka, O. A., Basler, K. and von Mering, C. (2011). Cell-sorting at the A/P boundary in the Drosophila wing primordium: a computational model to consolidate observed non-local effects of Hh signaling. *PLoS Computational Biology* **7**, e1002025.

Schwank, G., Dalessi, S., Yang, S.-F., Yagi, R., de Lachapelle, A. M., Affolter, M., Bergmann, S. and Basler, K. (2011). Formation of the long range dpp morphogen gradient. *PLoS Biology* **9**, e1001111.

Wu, C.-h. and Nusse, R. (2002). Ligand receptor interactions in the Wnt signaling pathway in Drosophila. *The Journal of biological chemistry* **277**, 41762–41769.

Wu, Y., Vendome, J., Shapiro, L., Ben-Shaul, A. and Honig, B. (2011). Transforming binding affinities from three dimensions to two with application to cadherin clustering. *Nature* **475**, 510–513.

Zhou, S., Lo, W.-C., Suhalim, J. L., Digman, M. A., Gratton, E., Nie, Q. and Lander, A. D. (2012). Free extracellular diffusion creates the Dpp morphogen gradient of the Drosophila wing disc. *Current biology : CB* **22**, 668–675.

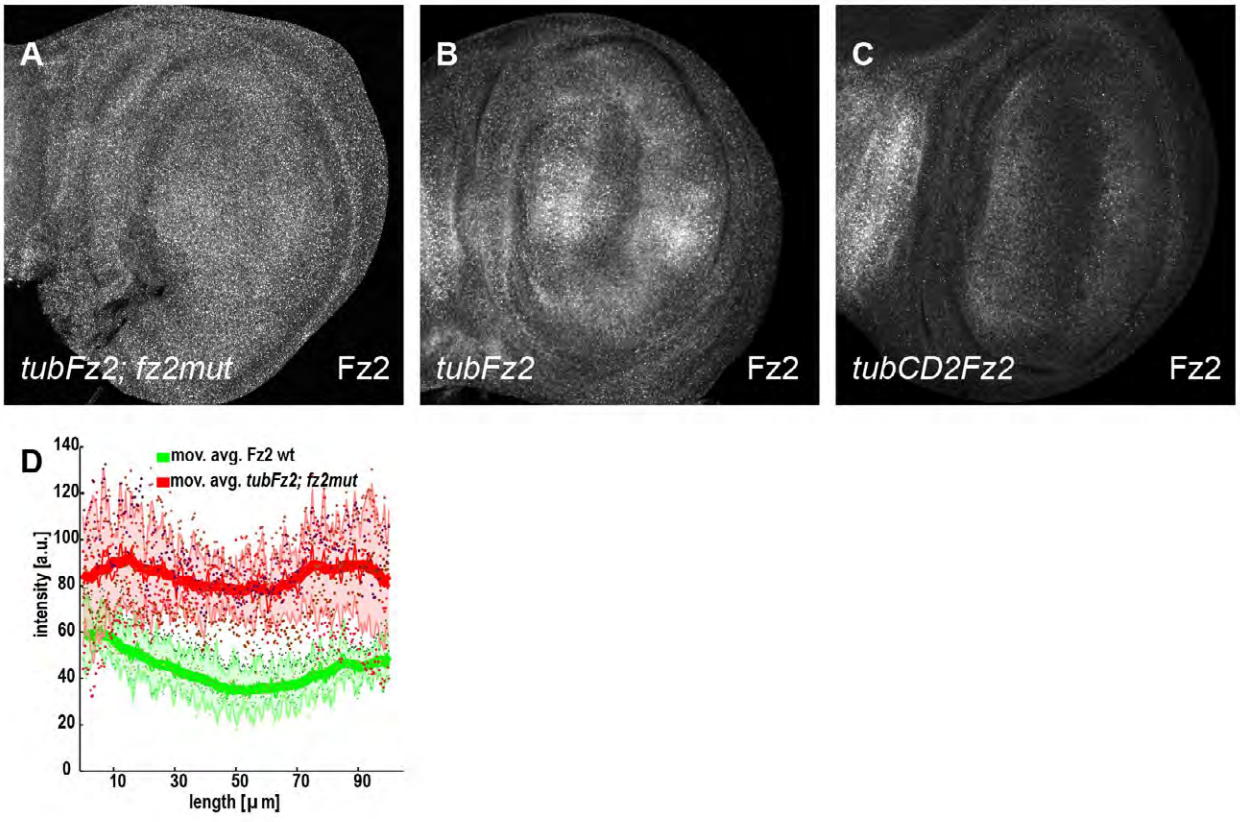

Figure S1: Fz2 gradient in *tubFz2* discs is maintained by endogenous Fz2 expression

Panel (A) shows a disc expressing the *tubFz2* transgene, but lacking all endogenous Fz2, thereby showing a weaker gradient of Fz2 expression. Panel (B) depicts a *tubFz2* disc with endogenous Fz2, while panel (C) shows a wild-type control. In (D) a maximum intensity projection of the receptor distributions of four wild-type and five *tubFz2*, *fz2*$^{-}$ discs are shown.

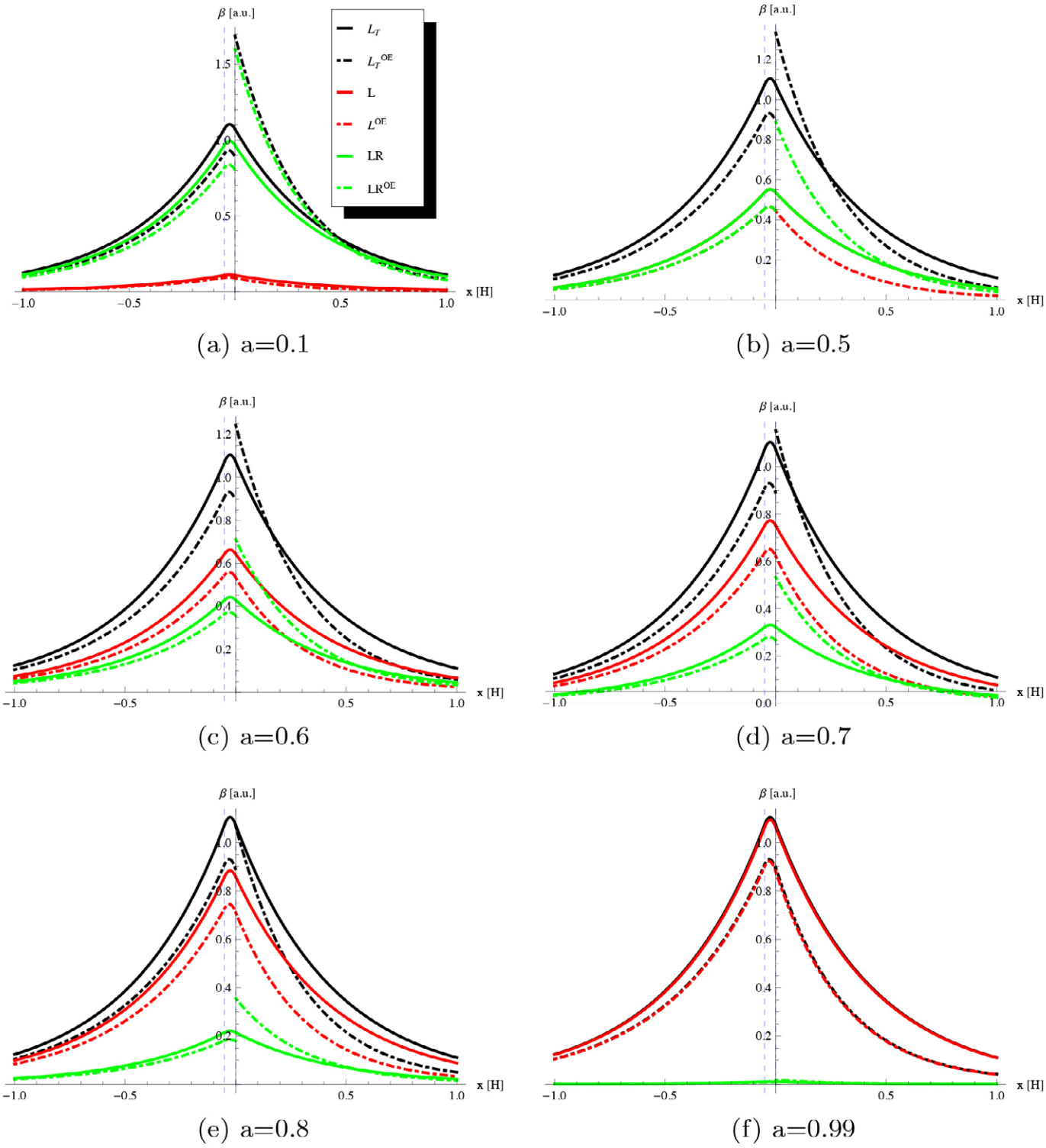

Figure S2: Comparison of Wg distributions in wild-type (x<0, solid lines) and receptor-overexpressing regions (x>0, dot-dashed lines) in a simplified model

We solved a simplified model of Wg-receptor interactions analytically (neglecting Fz3, no transcriptional receptor downregulation, no decay of unbound Wg)**.** To mimic Arr overexpressing experiments, we increased the amount of receptor by a factor n=2 for x>0 in graphs with dot-dashed lines. We show the total Wg (black), its free (red) and receptor-bound (green) components and vary the relative amount of free Wg, *a*. The Wg source is situated between $x_0 = -1/20 \times H$ (blue dashed line) and $x = 0$. The decay length of Wg is set to $l_{Wg} = 21\,\mu m$, the average wild-type decay length measured in discs, where Arr was compartmentally overexpressed. H indicates the half width of the region of interest of length $50\,\mu m$. Note the dependence of the increase in the amplitude of total Wg in the receptor-overexpression region on *a*.

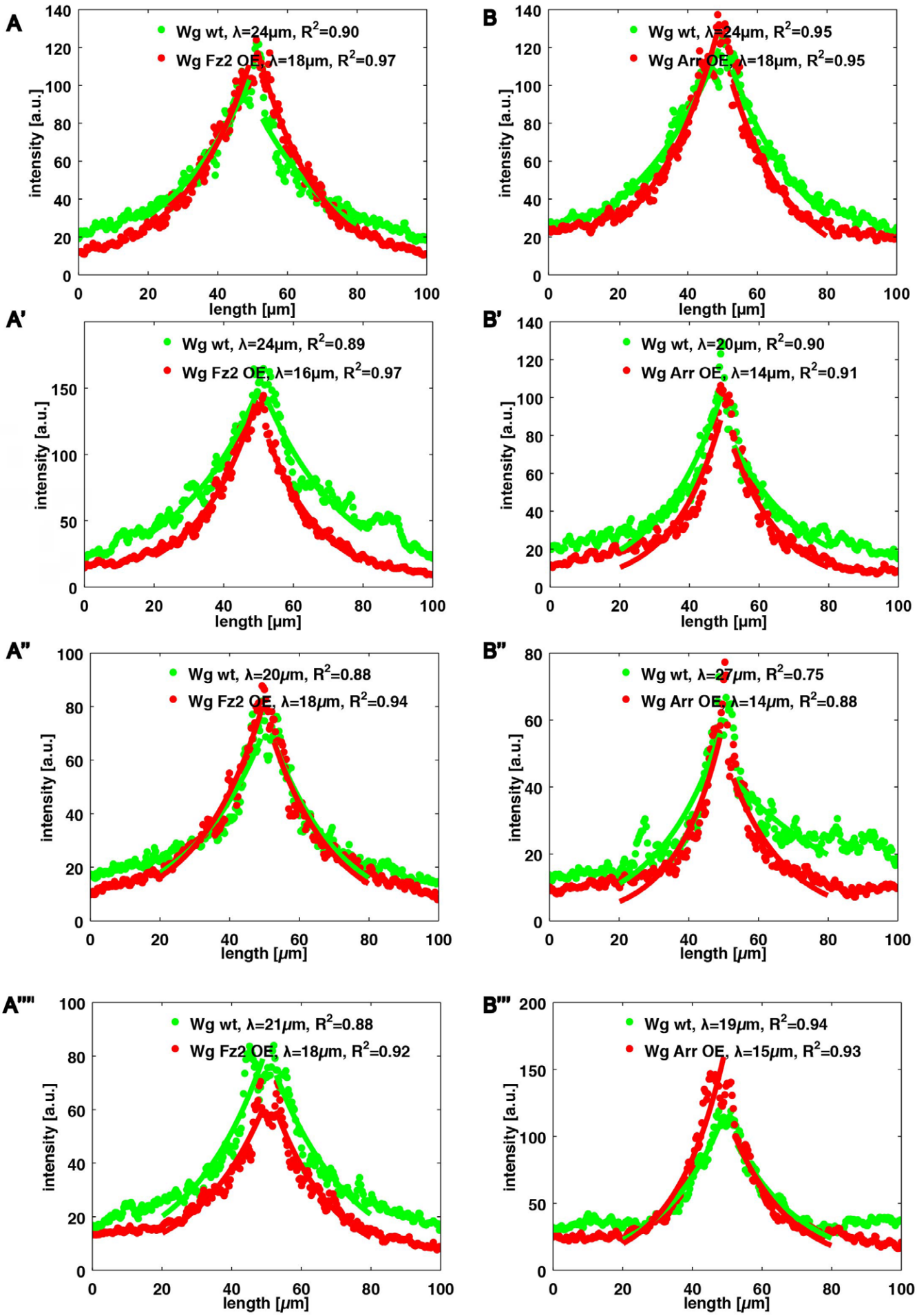
A
Wg wt, λ=24μm, R²=0.90
Wg Fz2 OE, λ=18μm, R²=0.97
intensity [a.u.]
length [μm]
B
Wg wt, λ=24μm, R²=0.95
Wg Arr OE, λ=18μm, R²=0.95
intensity [a.u.]
length [μm]
A'
Wg wt, λ=24μm, R²=0.89
Wg Fz2 OE, λ=16μm, R²=0.97
intensity [a.u.]
length [μm]
B'
Wg wt, λ=20μm, R²=0.90
Wg Arr OE, λ=14μm, R²=0.91
intensity [a.u.]
length [μm]
A''
Wg wt, λ=20μm, R²=0.88
Wg Fz2 OE, λ=18μm, R²=0.94
intensity [a.u.]
length [μm]
B''
Wg wt, λ=27μm, R²=0.75
Wg Arr OE, λ=14μm, R²=0.88
intensity [a.u.]
length [μm]
A''''
Wg wt, λ=21μm, R²=0.88
Wg Fz2 OE, λ=18μm, R²=0.92
intensity [a.u.]
length [μm]
B''''
Wg wt, λ=19μm, R²=0.94
Wg Arr OE, λ=15μm, R²=0.93
intensity [a.u.]
length [μm]

Figure S3: Narrowing of the extracellular Wg distribution upon receptor overexpression

Panels A-A''' show the extracellular Wg distribution in the posterior (displayed in red) and anterior (displayed in green) compartment of a single disc. In the posterior compartment, a *tubArr* construct was expressed by flipping out a *CD2* stop cassette via *hhGal4 UAS-Flp*. Panels B-B''' show the same, but here a *tubFz2* construct was used. We display the mean decay length λ and R^2 for the wild-type and receptor-overexpressing compartment of each disc. Fitting procedure as described in "Materials and Methods" section.

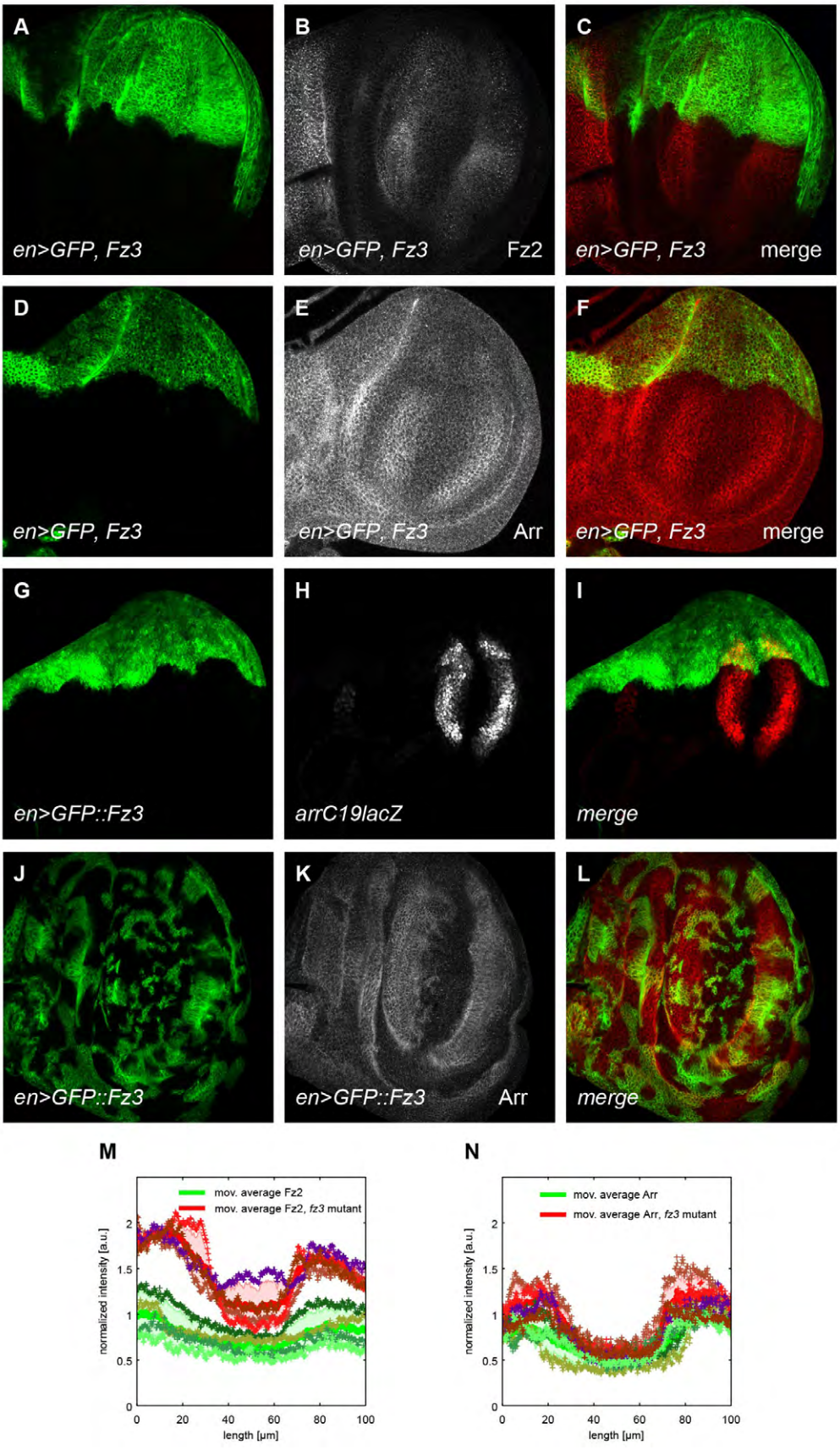

Figure S4: Fz3 downregulates Arr and Fz2 posttranscriptionally

Fz3 overexpression (green in A, D, G) in the P compartment reduces Fz2 levels (grey in B) and Arr levels (grey in E), but does not reduce *ArrC19* expression (G-I). In contrast, Arr protein levels are higher in Fz3 overexpressing clones away from the Wg source (J-L). Intensity profiles of Fz2 gradients (M) and Arr gradients (N) in *fz3* mutant (red) and wild-type wing discs (green). Note the higher intensity profiles of Fz2 and Arr in the *fz3* mutant wing disc.

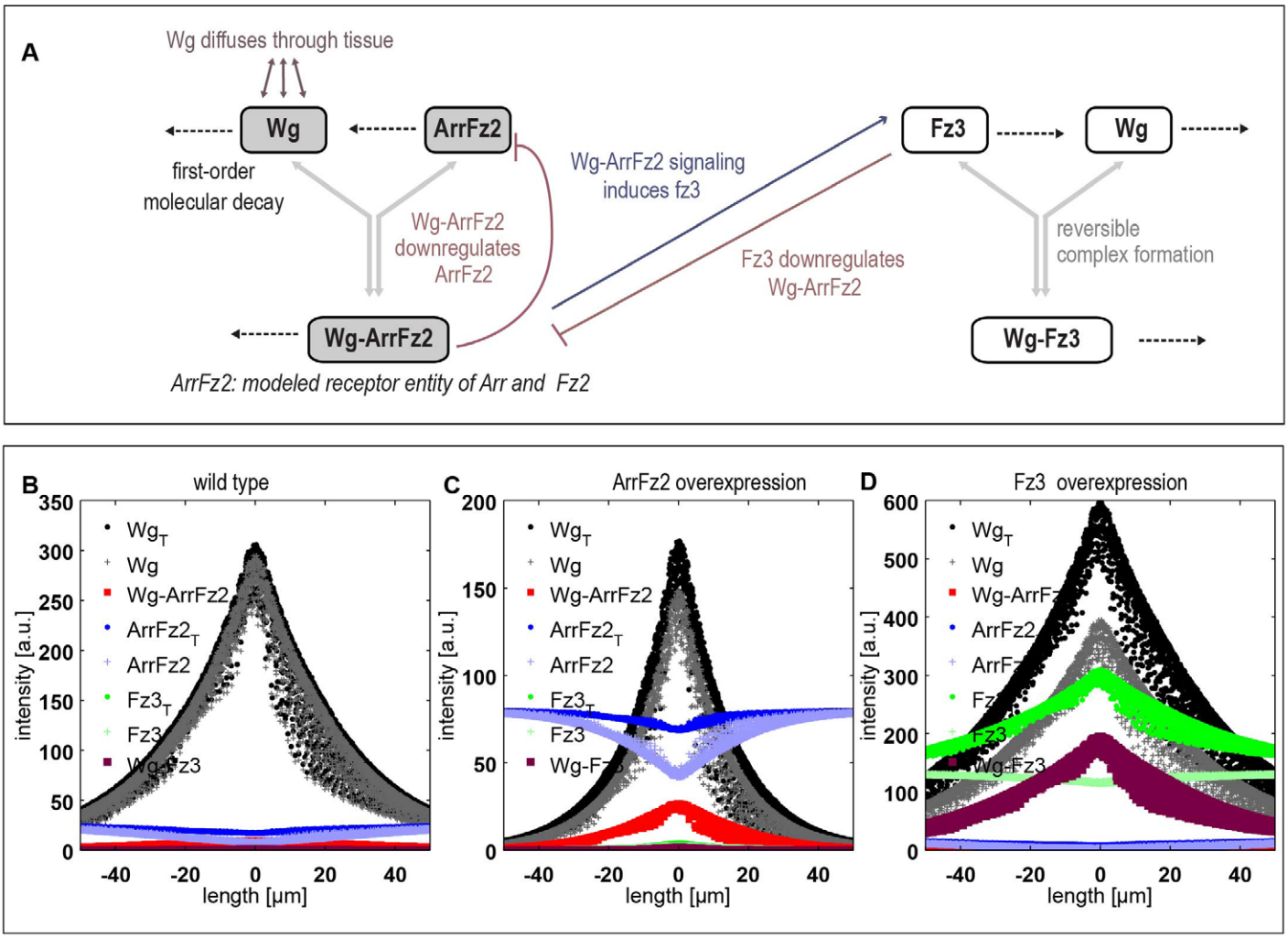

Figure S5: Model describing Wg signaling as the interplay of the two reversibly forming complexes, Wg-ArrFz2 and Wg-Fz3

In our extension of the original model (Fig. 2) the production of a second receptor Fz3 depends on Wg signaling (as modeled by the presence of the Wg-ArrFz2 complex). Fz3 itself attenuates Arr and Fz2 only in interaction with Wg. (B-D) Exemplary simulation run of full model with wild-type (B), ArrFz2 overexpression (C) Fz3 overexpression parameter sets (Table S2 of the Supplementary methods). Projection of the concentrations of all simulated players on the anterioposterior axis.

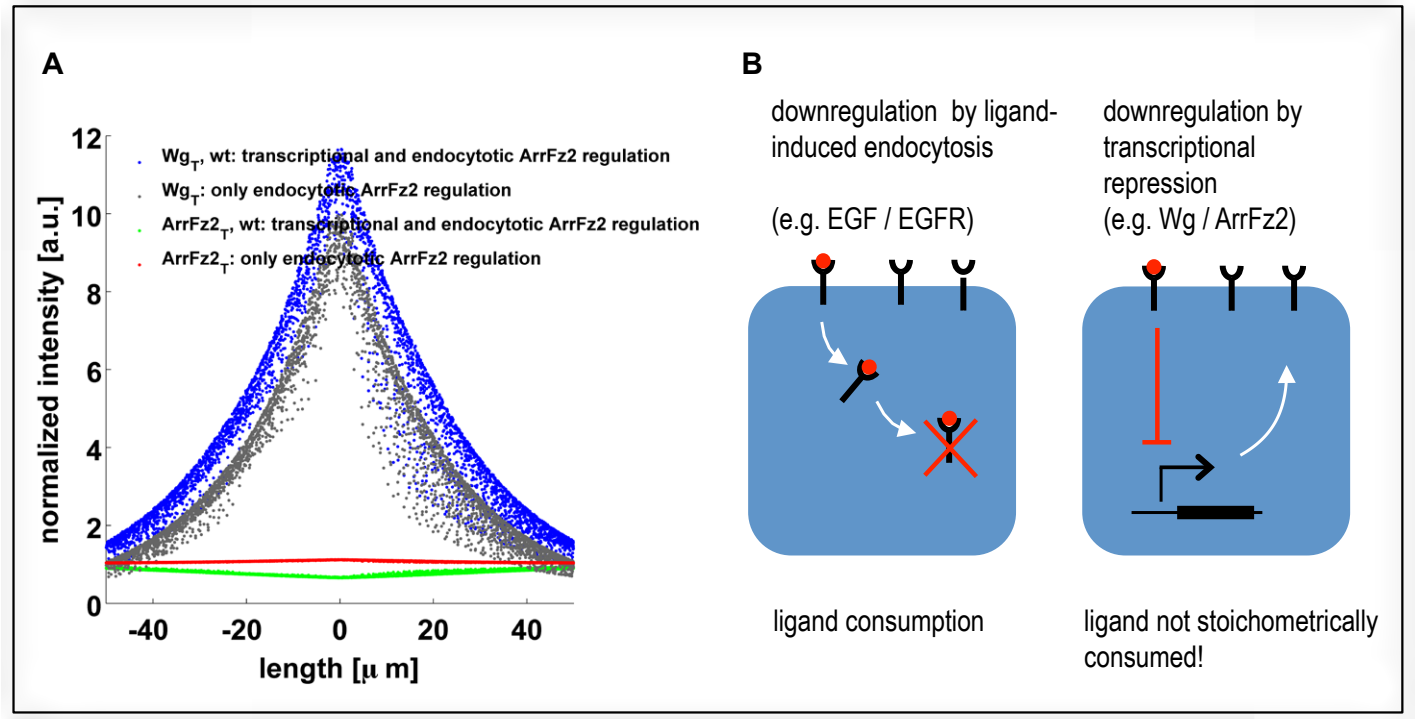

Figure S6: Transcriptional receptor regulation leads to broader Wg distribution

(A) We modeled purely endocytotic receptor downregulation (Wg distribution in grey, receptor distribution in red) by setting the Wg signaling induced transcriptional decay rate $k^t_{Wg\text{-}ArrFz2}$ in eq. (S.2) to 0. Note that with transcriptional receptor regulation, we observe a slightly broader Wg distribution and higher Wg amplitude (blue). (B) Schematic view of receptor downregulation by ligand-induced endocytosis vs. transcriptional repression.

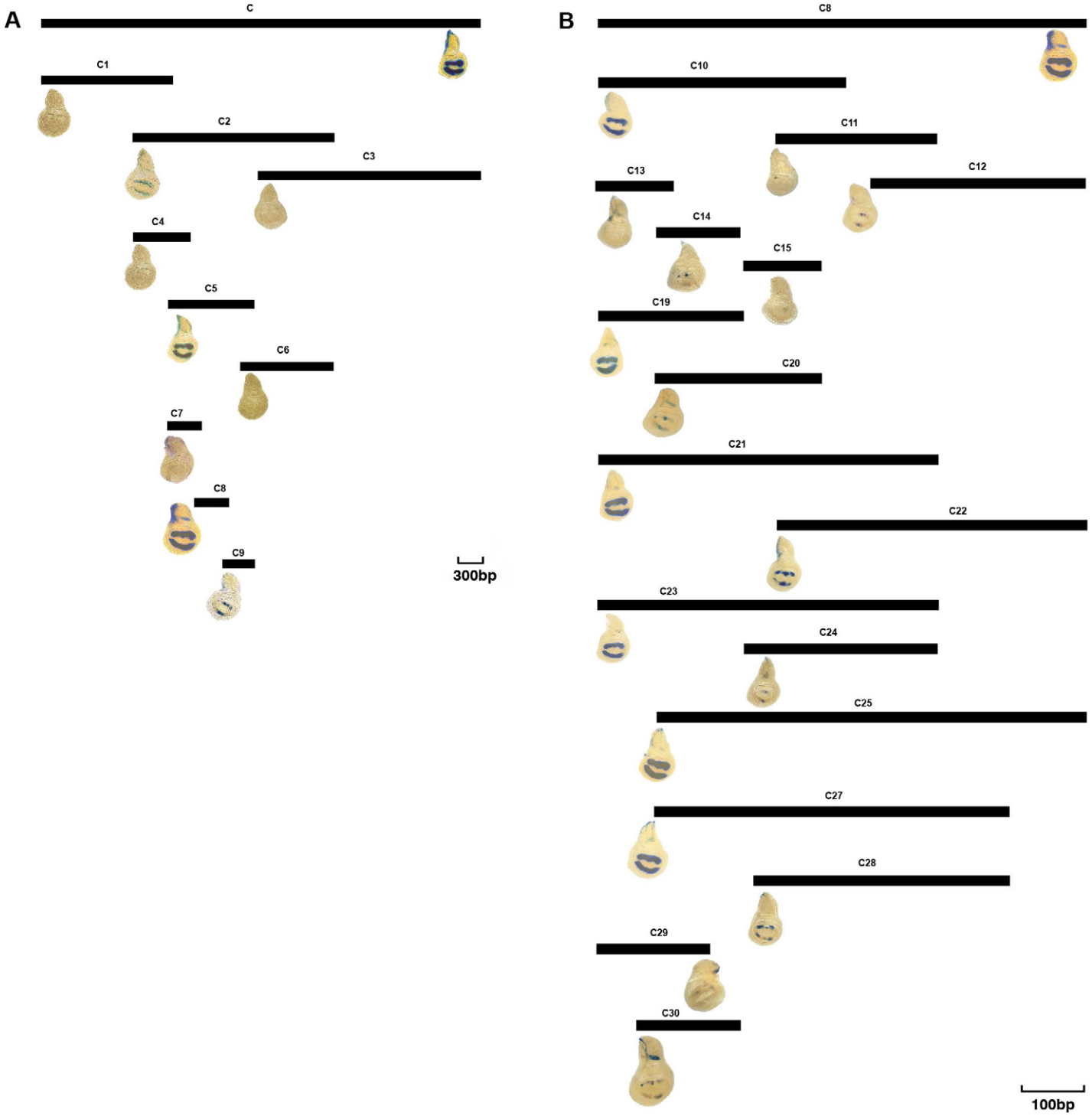

Figure S7: Dissection of the arr regulatory region

Panel (A) depicts the different genomic fragments from the *arr* regulatory region, which were cloned into a *lacZ* reporter vector and integrated into the same landing site on the second chromosome. Expression of *lacZ* in wing discs from third instar larvae is monitored by standard X-Gal staining assays. Dissection of the *arrC* enhancer results in *arrC8* and further narrowing down of *arrC8* yields the minimal enhancer *arrC19* (B).

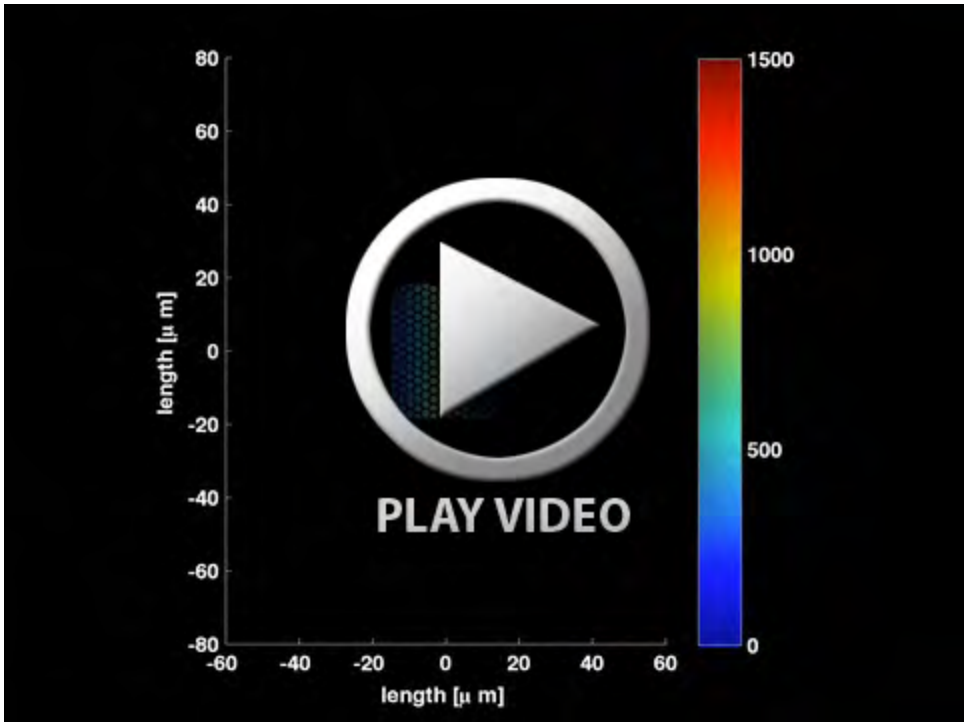

Movie 1: Total Wg distribution on a growing disc
We interchanged the simulation of the growth of the disc with the solution of the differential equations on the ever-changing cell topology (see Supplementary methods) for an exemplary parameter set. Note the increase in the Wg amplitude during the growth of the disc.

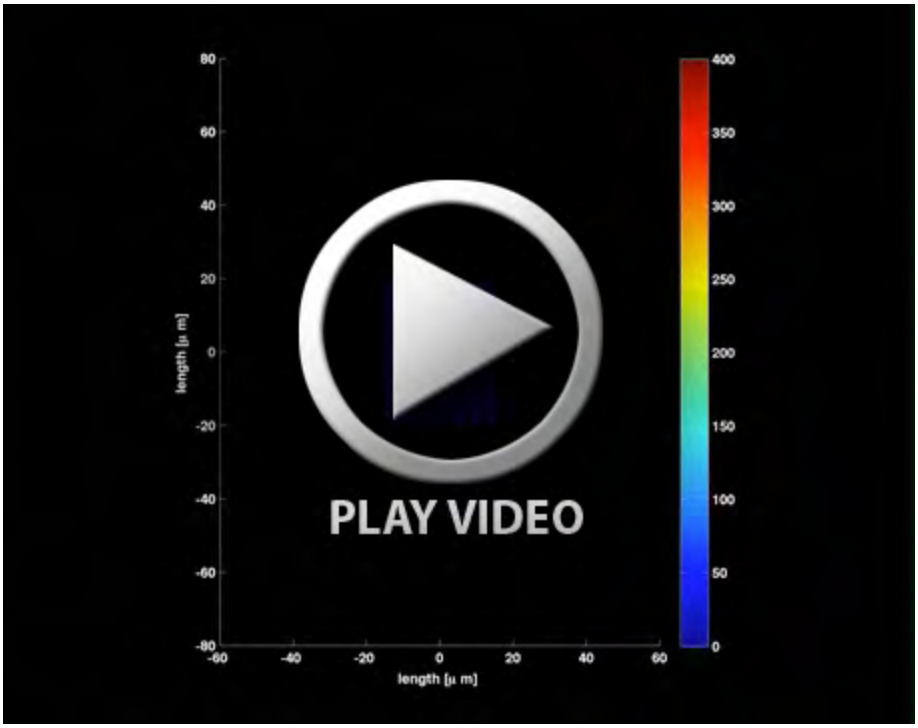

Movie 2: Total Arrow distribution on a growing disc

Table S1, Schilling et al.

Wg distributions: Exponential fits

Exponential fit of form $y = y_0 \cdot \exp(-x/\lambda)$, where
λ, y_0, R^2: mean decay length, mean amplitude and mean correlation coefficient of N discs

	λ [µm]	y_0 [a.u.]	R^2	N
Experiment				
Wg, wt	22 ± 2	113 ± 39	0.90	4
Wg, *tubFz2*	18 ± 3	107 ± 34	0.96	4
Wg, wt	21± 5	112 ± 26	0.89	4
Wg, *tubArr*	15 ± 2	117 ± 32	0.93	4
Wg, wt	35 ± 11	109 ± 42	0.74	9
Wg, *tubArrtubFz2*	26 ± 7	119 ± 52	0.81	9
Wg, wt	19 ± 11	66 ± 15	0.92	2
Wg, *tub Fz2; fz2mut*	18 ±4	72 ± 17	0.87	8
Wg, wt	23 ± 9	93 ± 20	0.85	4
Wg, *fz3*$^-$	21 ± 5	112 ± 16	0.81	4
Wg, wt	29 ± 5	39 ± 5	0.85	4
Wg, Fz3 OE	43 ± 13	81 ± 24	0.80	4
Simulation				
Wg, wt	23 ± 2	275 ± 41	0.90	10
Wg, ArrFz2 OE	14 ± 1	198 ± 30	0.89	10
Wg, Fz3 OE	38 ± 8	647 ± 86	0.87	10

Compartmental receptor mixexpression: Ratio of Wg amplitudes and decay lengths

Ratio of Wg amplitudes and decay lengths of the receptor overexpressing (OE) and wild type compartment are calculated for each disc, shown mean and standard deviation of N discs
p: p-value of hypothesis that amplitudes and decay length remain unchanged under receptor OE

	y_0^{OE}/y_0	p (y_0^{OE}/y_0-1)	$\lvert\lambda^{OE}/\lambda\rvert$	p (λ^{OE}/λ-1)	N
Experiment					
Wg, *tubFz2* / Wg, wt	1.0 ±0.1	0.42	0.8 ±0.1	0.0004	4
Wg, *tubArr* / Wg, wt	1.1 ±0.2	0.57	0.7 ±0.1	0.0002	4
Wg, *tubArrtubFz2* / Wg, wt	1.3 ± 0.3	0.30	0.8 ± 0.2	0.0020	9
Wg, Fz3OE / Wg ,wt	2.1 ± 0.7	0.05	1.3 ± 0.2	0.0390	4
Simulation					
Wg, ArrFz2 OE / Wg, wt	0.7 ± 0.1	$4 \cdot 10^{-8}$	0.61 ± 0.03	$2 \cdot 10^{-9}$	10
Wg, Fz3 / Wg, wt	2.4 ± 0.3	$6 \cdot 10^{-8}$	1.7 ± 0.3	$2 \cdot 10^{-5}$	10

Recptor distributions: Second order polynomial fit

Second order polynomial fit of form $y = ax^2+bx+c$; a b,c are the mean fit coefficients of N discs

	$a \cdot 10^5$ [a.u./µm2]	b [a.u./µm]	c [a.u.]	R^2	N
Experiment					
Fz2, wt	18 ± 4	-0.019 ± 0.004	1.1 ± 0.2	0.62	4
Fz2, *tubFz2*	34 ± 15	-0.036 ± 0.013	3.8 ± 0.4	0.48	4
Fz2, wt	18 ± 8	-0.018 ± 0.008	1.1 ± 0.3	0.78	4
Fz2, *fz3*$^-$	51 ± 16	-0.055 ± 0.018	2.6 ± 0.4	0.77	4
tubFz2; fz2mut	15 ± 22	-0.015 ± 0.021	1.7 ± 0.6	0.40	5
Arr, wt	27 ± 7	-0.025 ± 0.006	1.1 ± 0.3	0.84	4
Arr, *tubArr*	32 ± 17	-0.032 ± 0.015	2.4 ± 0.3	0.67	4
Arr, wt	33 ± 3	-0.031 ± 0.004	1.2 ± 0.2	0.80	4
Arr, *fz3*$^-$	49 ± 12	-0.048 ± 0.011	1.8 ± 0.3	0.79	4
Simulation					
ArrFz2, wt	18 ± 2	-0.00011 ± 0.00016	0.7 ± 0.0	0.85	10
ArrFz2, OE	42 ± 4	0.00019 ± 0.00014	2.7 ± 0.1	0.76	10

Table S1: Quantification of wild-type and receptor-misexpression Wg and receptor distributions in experiment and simulation

Experiment: We display the mean correlation coefficient $R^2 = \sum_{i=1}^{N} R_i^2$ of *N* measurements.
For Wg distributions, we display the mean of the absolute value of the decay length and amplitude. For receptor distributions we display the mean fit coefficients to a second order polynomial. In discs where the receptor misexpression was compartmental, we calculated furthermore the change in Wg amplitudes and decay length and displayed the mean of N measurements.
Simulation: Based on the parameter set given in Table S2 of the Supplementary methods, simulations were run on 10 different network topologies, containing between 4000 and 9000 cells. For each network topology, we projected the simulated concentration of total Wg and ArrFz2 of each cell on the anterio-posterior axis (example projection is shown in Figure 4). The extraction of the decay lengths followed the experimental fitting procedure described in the “Materials and Methods” section. All errors are standard deviations.